SKB

TECHNICAL REPORT 95-23

Spent nuclear fuel

A review of properties of possible relevance to corrosion processes

Roy Forsyth

Caledon Consult AB

April 1995

SVENSK KÄRNBRÄNSLEHANTERING AB
SWEDISH NUCLEAR FUEL AND WASTE MANAGEMENT CO
P.O.BOX 5864 S-102 40 STOCKHOLM SWEDEN
PHONE +46 8 665 28 00 TELEX 13108 SKB
FAX +46 8 661 57 19

SPENT NUCLEAR FUEL

A REVIEW OF PROPERTIES OF POSSIBLE RELEVANCE TO CORROSION PROCESSES

Roy Forsyth

Caledon Consult AB

April 1995

SPENT NUCLEAR FUEL

A REVIEW OF PROPERTIES OF POSSIBLE RELEVANCE TO CORROSION PROCESSES.

Roy Forsyth

Caledon Consult AB

April 1995

ABSTRACT

The report reviews the properties of spent fuel which are considered to be of most importance in determining the corrosion behaviour in groundwaters.

Pellet cracking and fragment size distribution are discussed, together with the available results of specific surface area measurements on spent fuel. With respect to the importance of fuel microstructure, emphasis is placed on recent work on the so-called structural rim effect, which consists of the formation of a zone of high porosity, and the polygonization of fuel grains to form many sub-grains, at the pellet rim, and appears to be initiated when the average pellet burnup exceeds a threshold of about 40 MWd/kgU.

Due to neutron spectrum effects, the pellet rim is also associated with the buildup of plutonium and other actinides, which results in an enhanced local burnup and specific activity of both beta-gamma and alpha radiation, thus representing a greater potential for radiolysis effects in ingressed groundwater. The report presents and discusses the results of quantitative determination of the radial profiles of burnup and alpha activity on spent fuel with average burnups from 21.2 to 49.0 MWd/kgU.

In addition to the radial variation of fission product and actinide inventories due to the effects mentioned above, migration, redistribution and release of some fission products can occur during reactor irradiation, and the report concludes with a short review of these processes.

SAMMANFATTNING

Rapporten ger en översikt över de egenskaper hos använt bränsle som bedöms viktigast för korrosionsegenskaperna i grundvatten.

Sprickbildning i bränslekutsar och samband mellan storleksfördelningar av bränslefragment och tillgängliga data för specifik yta hos bestrålat bränsle diskuteras. Beträffande bränslets mikrostruktur läggs tyngdpunkten på den så kallad rimeffekten, som består i bildning av en porös zon med ändrad kornstruktur vid randen av bränslet när bränslets medelutbränning överstiger cirka 40 MWd/kgU.

Rimeffekten är ett resultat av neutronspektrum och neutrontvärsnitt i bränslet, som ger ökad produktion av plutonium och andra aktinider vid randen av bränslet. Detta resulterar i ökad lokal utbränning och högre specifik aktivitet av såväl beta-gamma som alfa strålning, vilket kan ge ökad radiolys hos grundvatten. Rapporten presenterar och diskuterar resultat av kvantitativa mätningar av radiella fördelningar av utbränning och alfaaktivitet hos bränsle med utbränningar mellan 21.2 och 49.0 MWd/kgU.

Förutom inhomogeniteter i utbränning och aktivitetsinnehåll av ovannämnda skäl, diskuteras kortfattat även inverkan av omfördelning och frigörelse av fissionsprodukter under bestrålning. Rapporten avslutas med en kort sammanfattning av de olika mekanismerna.

TABLE OF CONTENTS

SUMMARY AND CONCLUSIONS

The use of the words **possible relevance** in the sub-title to this report does not imply that there is much uncertainty in identifying the main characteristics of spent nuclear fuel which are relevant to corrosion processes. These are, obviously, the structure of the fuel, including its surface area, and the heterogeneities of distribution of its components, actinides, fission products, impurities and including oxygen. Heterogeneity, here, is defined as the variation of concentrations over the fuel pellet radius due to neutron spectrum effects, or more local redistribution effects due to processes such as thermal diffusion, grain boundary sweeping and mass transport, or by chemical reactions and solubility limitations.

The term spent fuel, however, covers fuel with a wide range of those properties which are determined by fuel temperature and irradiation history, and work during the last few years on structural changes and actinide concentrations at the fuel pellet rim, has broadened this range. At the present time, it is uncertain whether, or to what degree, several of these fuel characteristics have an effect on the corrosion properties of spent fuel. The aim of this report is to review the current state of knowledge based on experimental data on spent fuel characterization, and, since the reference fuels in the SKB spent fuel corrosion programme have burnups roughly representative of average discharge burnups, published and unpublished results from their characterization have been used to illustrate the effects.

Many of the spent fuel corrosion experiments which have been performed, or are in progress, in national programmes in countries such as Canada, Germany, Sweden and the U.S.A., have been designed with these questions in mind, but discussion of the available results is not included in this report.

With respect to the surface area of spent fuel, very few experimental values have been published, and the report presents recent results on two of the reference fuels used in the SKB experimental corrosion programme. The specific surface areas of these fuels, fuel pellet fragments removed directly from the clad, as determined by the BET method using Kr, were in the range 70-120 cm^2/g. These values are larger than the calculated geometrical surface areas, and, assuming a surface roughness factor of 4, it is estimated that gas penetration into the fuel fragments occurred to a depth of 6 or more fuel grains through inter-granular porosity. For spent fuel corrosion, it is important to determine whether continuing corrosion will increase this penetration depth or whether the precipitation of corrosion products will hinder water access.

Emphasis in the report has been placed on discussion of the so-called pellet rim effect, where the formation of a high porosity zone, and the loss of fuel structure involving the formation of many sub-grains, represent a potential

increase in surface area exposed to ingressed water during corrosion. Also, the formation of the sub-grains may be associated with a redistribution of leachable components to the surface. The two effects are not coincident, since in the fuels discussed in the report, the porous zone was shown to be only 20-40 microns broad, while sub-grain formation was observed several hundreds of microns into the fuel.

Although a threshold value of average pellet burnup of about 40 MWd/kgU (corresponding to a local burnup at the rim of about 65 MWd/kgU) is given here for the formation of the porous zone, it is not yet established that burn-up is the only parameter; other fuel parameters, for example, the irradiation history and fuel/clad contact may be of importance.

The report also presents the results of measurements of the radial profiles of burnup and alpha activity on the SKB reference fuels. The **formation** of a pellet rim zone of enhanced alpha activity occurs in all LWR UO_2 fuels, since it is not burnup related. The specific alpha activity and actinide composition at the rim, however, are strongly dependent on the burnup, and the results presented for two fuel pellets from the same rod, (i.e., with fairly similar irradiation histories) with burnups of 21.2 and 49.0 MWd/kgU, show that there was a factor of about 6 between the specific alpha activities at the pellet rims.

The positional coincidence between the porous zone and the enhanced alpha activity at the pellet rim represents an increased potential for corrosion by alpha radiolysis induced oxidation. Currently, however, the experimental data is insufficient to establish whether, in general, the pores at the pellet rim are open or closed in spent fuel, or whether the amount of connected porosity is dependent on burnup or other irradiation parameters. Hopefully, work in progress on the mechanisms for pore and fuel sub-grain formation at the pellet rim, together with results from on-going corrosion tests will bring more clarity to the problem.

The report also discusses recent work on the determination of the local fuel oxidation potential of spent fuel, particularly at the pellet rim where changes in potential could be expected due to the increased fraction of fission in Pu isotopes. The conclusion reached on the basis of the experimental results was that the fuel remained essentially stoichiometric, while excess oxygen was consumed either by clad inner-wall oxidation, or by oxidation of fission product molybdenum.

Finally, the report discusses briefly the question of fission product segregation, and concludes that it is difficult by means of post-irradiation examination techniques to define quantitatively the amount and distribution in the pellet of such segregations.

1. INTRODUCTION

According to the most recently published estimation (1), the accumulated amount of spent nuclear fuel produced in the Swedish nuclear power programme up to the year 2010, will be about 7 800 tons, of which the subtotals for BWR and PWR fuel are 5 900 tons and 1 800 tons respectively.

The accumulated totals of spent BWR and PWR fuel up to and including 1994 were 2 300 and 700 tons. The fuels in these two categories, however, were supplied by a number of fuel vendors, and , more importantly, represent the results of over 30 years of continuous development of LWR fuel and, therefore, display significant differences in properties.

Fuel vendors and the nuclear power utilities have performed extensive fuel testing and development programmes aimed at improving the safety and reliability of nuclear fuel, partly in response to a variety of fuel defection modes observed over the years, including inner clad wall hydriding, clad collapse due to fuel densification, and clad failure due to pellet/clad interaction (PCI) and stress-corrosion cracking (SCC).

In addition to improvements in fuel production and quality control, major changes in design at the pellet, fuel rod and assembly level have been successively introduced. These have included rod pre-pressurization to reduce clad creep-down and the deleterious effect of fission gas release on heat transfer over the pellet/clad gap, the introduction of modified clad types (e.g., liner, low corrosion), and smaller pellet and fuel rod diameters. In Sweden, this latter design change has resulted in modern BWR assemblies with 10 x 10 fuel rod arrays compared with the earlier 8 x 8, while PWR assemblies consist of a 15 x 15 array (Ringhals 2) while a 17 x 17 array is used in Ringhals 3 and 4. An interesting consequence of these developments is that pellet design has tended to converge for BWR and PWR fuels.

The smaller pellet diameters improve fuel performance in that fuel temperatures are significantly reduced for a given linear heat rating, which reduces pellet/clad mechanical interaction, and fuel restructuring with associated release of fission gases and volatile fission products (including iodine which is known to cause SCC).

The marked improvement in fuel performance has permitted a gradual extension of discharge burnup without loss of reliability such that average burnups are currently about 40 MWd/kg U for both BWR and PWR fuel, an increase of about 30% over the past 15 years.

It is clear from the above that the spent fuel already discharged from the Swedish reactors displays an appreciable range of those properties determined by fuel temperature and burnup. Since fuel development efforts

continue, it is likely that further design improvements will be introduced in the future.

There is an abundant literature on the **detailed** characteristics of fuel irradiated to a wide range of burnup and power levels, and reports of extensive characterization work on spent fuel selected specifically for corrosion tests, for example in the programmes in Sweden (2) and the U.S. (3-7), have been published.

In this report, therefore, attention is directed primarily to those characteristics of spent fuel which are of generic nature, and with emphasis on the results of research performed during the last decade which has been concerned with structural and associated effects observed in fuel of moderate to high burnup. Such information, of course, is of great value for the design of experiments for the study of corrosion processes in spent fuel, and for their evaluation.

Where possible, the results obtained on the reference spent fuels in the SKB programme are used to illustrate the observed effects. This has also given the opportunity to present a number of hitherto unpublished results obtained during fuel characterization work in the Studsvik Hot Cell Laboratory, including some from the last year.

The 3 main fuels used in the programme are:

- BWR Reference Fuel. Fuel rod O1-418-A6 from the first reload for the Oskarshamn-1 BWR. Irradiated 1972-1979. The fuel used for characterization and in the corrosion tests had an average burnup of 42 MWd/kgU. The measured integral fission gas release for the rod was 0.7%.

- PWR Reference Fuel. Fuel rod D07-03688 from the Ringhals-2 PWR. Irradiated 1977-1983.The fuel used for characterization and in the corrosion tests had an average burnup of 43 MWd/kgU. The measured integral fission gas release for the rod was 1.05%.

- Variable Burnup/Linear Heat Rating Fuel. Lower rod segment 79B2 of segmented rod 5830 G2 from the Ringhals-1 BWR. Irradiated 1979-1987. This rod had a burnup gradient from about 20 to 49 MWd/kgU. The measured integral fission gas release for the rod was 1.1%.

2. FUEL STRUCTURE

2.1 FUEL PELLET CRACKING

On reactor startup or shutdown, the sintered fuel pellets fracture due to thermal stresses, forming a number of radial and roughly circumpherential cracks. As can be clearly seen on inspection of macrographs of fuel cross-sections, the cracking pattern can vary significantly even in adjacent pellets in the pellet stack. Although it could be expected to depend to some extent on the irradiation history and burnup, such a relationship has not been quantified.

In general, however, the fuel fragments consist largely of irregular wedges, usually bounded by the pellet periphery and radial cracks. Fig.2-1 shows the fuel fragments removed from a 40 mm long section of the BWR reference fuel.

Since the microstructure of spent fuel, for example with respect to grain size and porosity, varies across the pellet radius, the specific surface area of the fragments could also reflect this variation. As a first step in investigating this possibility, the fragment size distributions of fuel removed from short sections of the BWR and PWR reference rods were determined by sieving. The samples were taken from the same parts of the rods (and therefore had similar burnups and irradiation histories) as the specimens used in corrosion testing.

Figure 2-1. *Fuel fragments from the BWR reference fuel. (x 3)*

For the BWR fuel, the size fraction measurements were performed on fuel samples from two positions in the rod, and showed good agreement. The weight percentages of the size fractions for the two reference fuels are presented in Table 2-1.

Table 2-1. Fuel fragment size distribution.

	Weight %				
Size fraction	> 4mm	4 - 2mm	2 - 1mm	1 - 0.5mm	< 0.5mm
BWR reference fuel	64.7	31.1	3.0	0.8	0.4
PWR reference fuel	23.8	68.7	4.7	1.9	1.0

There is some uncertainty in the values for the 2 smallest size fractions since they can contain a contribution from fragments produced during cutting out the samples. However, it is clearly seen that over 90% of both fuels consisted of fragments larger than 2mm, and for the BWR reference fuel fragments about 65% were larger than 4 mm. It should be noted that the PWR fuel pellets had a smaller diameter (9.1mm) than the BWR pellets (10.4mm) and that most of the "peripheral" PWR fuel wedges were retained in the 2-4 mm fraction.
Although the size distribution values given in the table are strictly only valid for the fuel samples examined, it is probable that they are broadly representative of spent fuel, and can be used for rough calculation of the surface area of the fuel presented for corrosion by ingressed water. This will be discussed further in section 2.3.

2.2 THE PELLET/CLAD GAP AND CRACK VOLUME

When the pellet cracks open during reactor power operation, the fuel fragments move radially outwards towards the clad, thus reducing the fabricated pellet/clad gap, and even after reactor shutdown, some of this outward relocation of the fragments is retained.
During continued irradiation, other processes, such as fuel swelling due to increasing fission product inventories, and clad creep-down (PWR) caused by the system pressure, result in a permanent decrease in the free volume in the rod, and eventually in pellet/clad gap closure at power. Before this stage is reached, the fuel fragments can "lock" together near the clad and thus impede axial gas transport in the rod. This has significance for the distribution of free volume between the residual gap and the fuel cracks, and also for thermal feedback effects locally in the rod during reactor operation.
These feedback effects can be initiated by local fission gas release due to a power increase or control rod movements. Locking of the fuel fragments impedes gas transport, resulting in local pollution of the helium filler gas with Kr and Xe and associated deterioration of heat transfer between fuel and clad. The fuel temperature rises, with further fission gas release and reduced heat transfer.
Clearly, the total cold free volume in a fuel rod, and its distribution between the residual fuel/clad gap and the inter-fragment cracks, are dependent on

fabrication parameters, burnup and irradiation history, and can also vary significantly along an individual rod.

Information on the free volume in the rod at a given pellet position can be obtained by means of a compression test (8,9) where the rod is compressed transversely between two 10 mm wide flat edges until hard contact is obtained between the pellet fragments and the clad. From the slope changes in the measured stress-strain curve two values of the residual diametral gap can be derived; the first, defined as relocated pellet, is considered to represent the position when the pellets fragments have been compressed inwards to reform the cracked pellet, while in the second, defined as compressed pellet, the pellet fragments have been further compressed to convert the inter-fragment gaps to an equivalent diametral gap.

Such measurements have been performed on the fuel rods used in the SKB Spent Fuel Corrosion Programme performed in the Hot Cell Laboratory of Studsvik Nuclear AB. The results on the PWR reference fuel rod are given in Figure 2-2. The compression test was only applied over the metre-long rod section from which the specimens for fuel characterization and corrosion testing were taken, and the locations of the measurement points were selected to avoid the test specimen zones.

Profilometry measurements on the rod (2) showed that the diametral clad creepdown at these positions was of the order of 50 microns. Inspection of Figure 2-2 shows that the residual pellet fragment-clad diametral gap (relocated pellet) had an average value of about 35 microns, with appreciable scatter, while the diametral gap equivalent to the inter-fragment cracks (compressed pellet) was about 50 microns. This latter value must be "shared" between the pellet cracks (Figure 3-1 shows the cracking pattern of

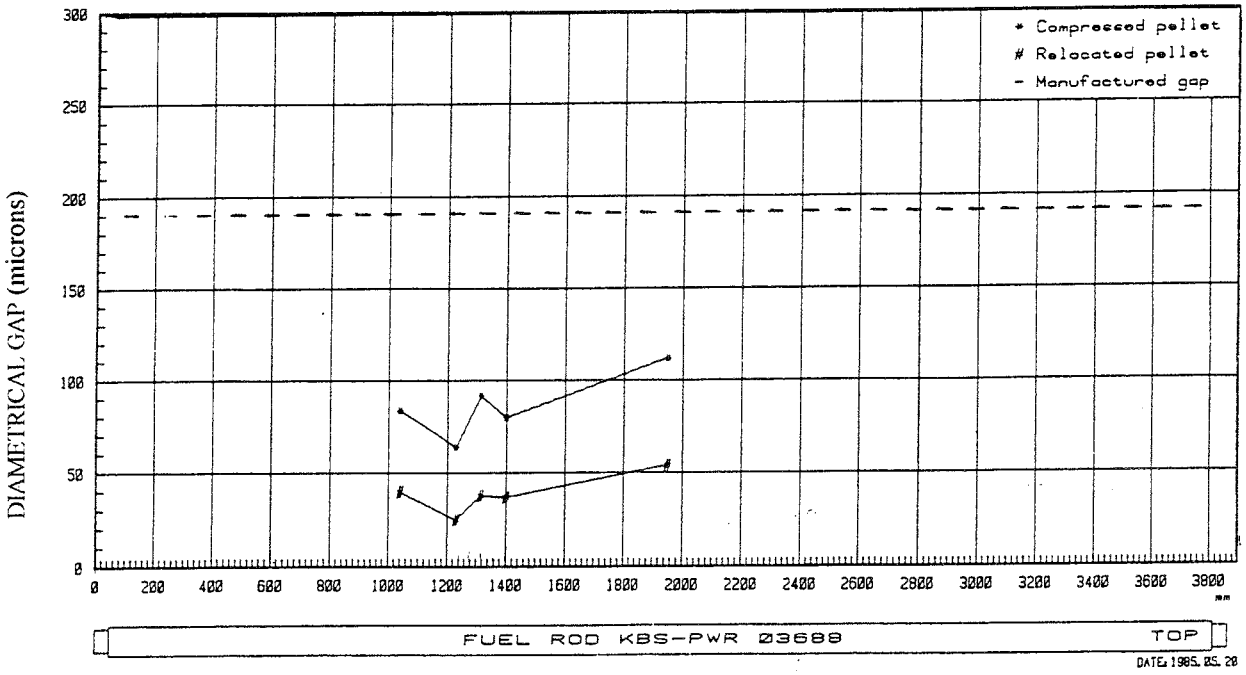

Figure 2-2. *Fuel/clad gap measurements on the PWR reference fuel rod.*

the PWR fuel ceramography specimen) which suggests that after possible water ingress to the rod, all water-filled gaps, including the pellet-clad gap, **on average**, are somewhat smaller than alpha particle ranges, which is of significance for possible fuel oxidation effects due to alpha radiolysis.

Clad compression measurements were also performed on the BWR reference fuel rod at 200 mm intervals along the pellet stack, avoiding assembly grid positions. Here, no clad creepdown had occurred, and the measured values of the residual diametral gap given below can be compared with the fabricated pellet/clad gap of 180 microns. The mean and standard deviation of the 9 measurement points over most of the fuel column (burnup 38 - 42 MWd/kgU) were;
Relocated pellet: 46 +/- 21 microns. Compressed pellet: 96 +/- 21 microns.
Thus the BWR and PWR reference fuels had similar inter-fragment free volumes, but the BWR fuel had a somewhat larger residual pellet fragment/ clad gap.

2.3 FUEL SURFACE AREA

The surface area of the fuel which would be available for corrosive attack by ingressed groundwater is an essential parameter for determining the corrosion rate. Unfortunately, the literature contains only a few references to surface area determination on unirradiated UO_2, and even fewer on spent fuel. A further difficulty is the unambiguous definition of spent fuel surface area in the context of the structural features of the fuel (fragments, grains and porosity) and the methodology employed for its measurement.

Because of these difficulties, it has been the practice to present the results of semi-static corrosion tests on spent fuel, as fractions of the total fuel inventory of a particular nuclide released to the aqueous corrodant during the test. This is an unambiguous value, being based on analytically-determined quantities, and is useful for comparison between fuels with different irradiation histories, for tests with different corrodants and at different temperatures, and to the study of its variation with fuel/corrodant contact time. The method has the advantage of permitting corrosion tests on relatively large samples which are representative of pellet cross-sections, thus including radially-varying properties such as fuel structure, possible fission product segregations, and inventories. The semi-static test is also a reasonably close analogue of the real situation after water ingress to the rod, but, in the absence of surface area data, cannot be used for absolute rate determinations.

Spent fuel fragments of size 4 mm from the reference BWR and PWR fuels (as seen from Table 2-1, this size represents a significant weight fraction of spent fuel) would contain, respectively, about $7.7\ 10^7$ and $1.8\ 10^8$ individual fuel grains, assuming cubic form for both fragments and grains. Clearly, the surface area exposed to corrodant contact will be dependent on the degree of grain boundary porosity and its inter-linkage, and would therefore be expected to vary with fuel burnup and irradiation history.

As mentioned above, the BET method for surface area determination, often employing krypton as the adsorbed gas, has been applied to the measurement of surface areas of sintered (i.e., prepared from fuel pellets) samples of both unirradiated UO_2 and spent fuel of various types, burnups and irradiation history. The available values of specific surface area of different size fractions are collected in Table 2-2. It should be noted that each size fraction range is fairly broad, and has an unknown size distribution within the range. The values are also plotted in Figure 2-3, where the results for the unirradiated material are plotted as dashed lines, and those for spent fuel as solid lines. The figure also includes for comparison a plot of the variation of the specific surface areas of idealized spheres and cubes as a function of diameter or cube side, and a parallel line (legend RF: 4) where an arbitrarily-selected roughness factor of 4 has been applied.

The results for the size fractions of fragments of crushed and sieved unirradiated UO_2, and for the > 4mm and 2 - 4mm fragments of the SKB reference BWR and PWR spent fuels, both show, as expected, large deviations from the calculated lines due to the effects discussed above. It should be noted that the results on these spent fuels are from an on-going BET measurement programme which also contains fuels of higher and lower burnups, and with different values of fission gas release. The comments below, therefore, may be complemented and modified when all results are available.

Although there is uncertainty, probably unresolvable, whether BET surface area results obtained by krypton adsorption are representative of the surface areas of spent fuel exposed to aqueous corrodants in laboratory corrosion tests performed at atmospheric pressure, or in deep geological repositories, they are the only values practically available. A rough test of their applicability, however, can be performed by estimating the average krypton penetration depth in the fuel fragments by comparing the measured surface areas with the calculated surface area of individual fuel grains based on ceramographic measurement of grain size.

By means of normalized weight fractions from Table 2-1, (the size fractions < 2 mm are ignored), and the BET results in Table 2-2, the preliminary bulk-averaged surface areas of the BWR and PWR reference fuels can be calculated to 78.9 and 85.5 cm^2/g respectively. The true grain sizes for these fuels were about 9.4 and 7.1 microns. (See section 2-4) Considering a 4 mm cubic fuel fragment, and assuming cubic grains with a roughness factor of 4, and that 3 of the grain sides are fully exposed to corrosive attack, the average depth of penetration for the BWR and PWR reference fuels can be calculated to 6.8 and 6.1 layers of grains respectively. If interlinkage is effected by grain edge porosity, these values could be somewhat larger.

As stated above, these are rough estimates, but the calculated penetration depths are conceptually acceptable, and it is suggested here that the BET surface area results for fuel fragments can be used for corrosion rate calculation, even with the validity restrictions discussed above.

Table 2-2. Specific surface areas (BET) of unirradiated UO_2 and spent fuel.

Unirradiated UO_2			Spent Fuel			
Size fraction (microns)	Surface area (cm^2/g)	Ref.	Burnup (MWd/kgU)	Size fraction (microns)	Surface area (cm^2/g)	Ref.
< 44 *	3700	10	50	7 - 20 *	2770	14
44 - 105 *	270	11	42	> 4000 **	59	13
100 - 300 *	113	12	42	2000 - 4000 **	121	13
500 - 1000 **	98	13	43	> 4000 **	79	13
500 - 1000 **	105	13	43	2000 - 4000 **	88	13
900 - 1100 *	160	12	43	All **	72	13
1000 - 2000 **	55	13				
1000 - 2000 **	80	13				
2000 - 4000 **	44	13				
Whole Pellet	150	10				

* Crushed and sieved. ** Fuel fragments

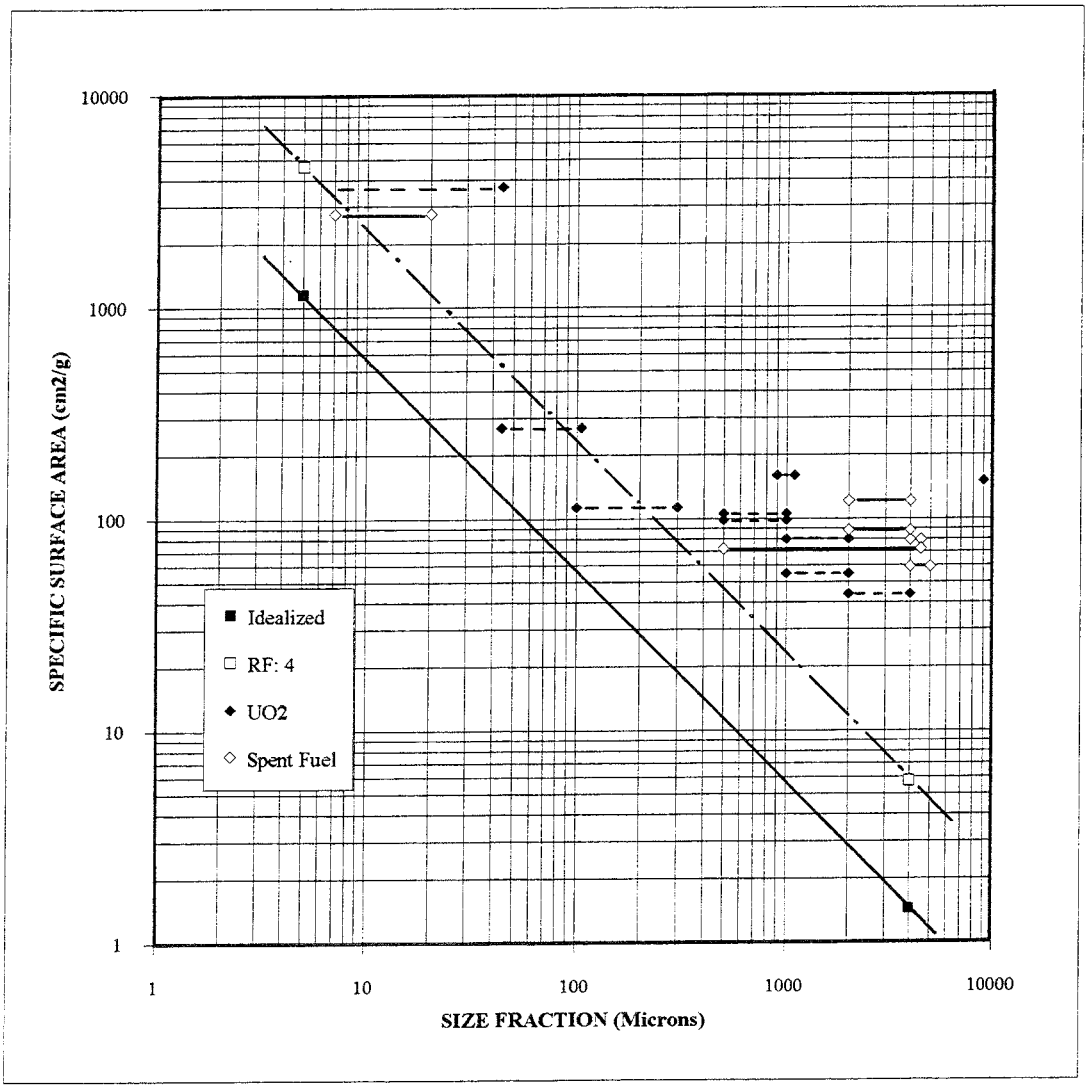

Figure 2-3. *Specific surface area (BET) of various size fractions of unirradiated UO_2 (dashed lines) and spent fuel (solid lines) as a function of size fraction.*

2.4 THE PELLET RIM EFFECT

Athough it is clear from the previous section that the grain size and fuel porosity can be of importance in determining the surface area of spent fuel exposed to corrosion, as was stated in the Introduction of this paper, they will not be discussed in detail here because of the wide range of values observed in spent fuel of different fabrication, burnup and irradiation history, and as a function of radial position.

For the relatively low temperature LWR reference fuels used in the SKB spent fuel corrosion programme, both grain size and porosity show little radial variation over most of the pellet radius. The post-irradiation characterization of the PWR reference fuel (2) showed, for example, that at a pellet radius of 4 mm, about 500 microns from the pellet rim, the grain size (AIL: average intercept length) of 4.3 microns was very similar to the as-fabricated structure, while at the pellet centre, some grain growth had occured to give grains of about 5.7 microns (AIL). The corresponding values for the BWR reference fuel were 5.5 and 6.5 microns. It can be noted here that for the discussion on surface area in section 2.2, average grain sizes (AIL) of 4.5 and 6.0 microns were used for the PWR and BWR fuels, giving, on correction with a factor of 1.57 (15), true grain sizes of 7.1 and 9.4 microns respectively.

The radial variation and size distribution of porosity in the PWR fuel has been reported in detail (2). The radial variation of total porosity in the BWR reference fuel is presented in Figure 2-4.

Here, the porosity measurements show a steep increase near to the pellet periphery. This is due to the so-called pellet rim effect, which has attracted great interest during the last few years, since the fuel microstructure shows very large modifications with respect to the local porosity (increased) and the grain size (substantially diminished) in a peripheral zone.

For the in-reactor performance of nuclear fuel, this may be of some significance for fuel properties such as fission gas release, fuel swelling and thermal conductance. Obviously, the effect may be also of significance for spent fuel corrosion.

Figures 2-5 and 2-6 present SEM photomosaics of part of the rim zones of the BWR and PWR reference fuels. The high porosity zones in both fuels, which have about the same burnup, appear to

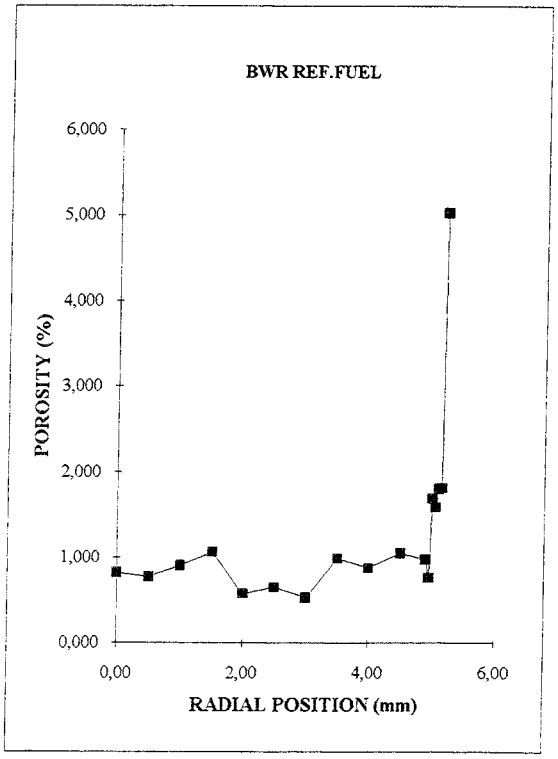

Figure 2-4. *BWR reference fuel.* Radial variation of porosity.

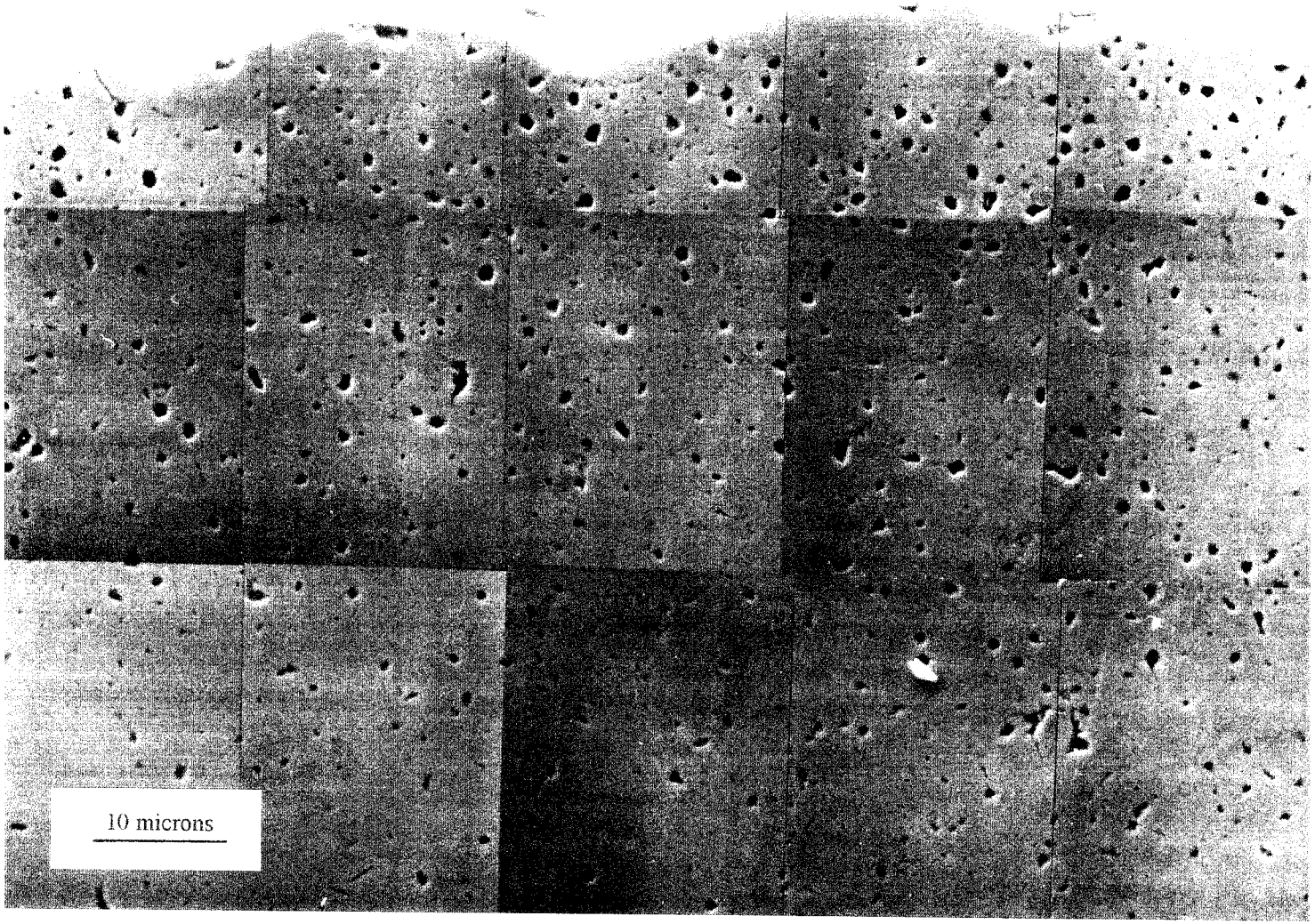

Figure 2-5. BWR reference fuel: (Burnup 42.0 MWd kgU) Pellet rim zone. Polished surface (x 2000)

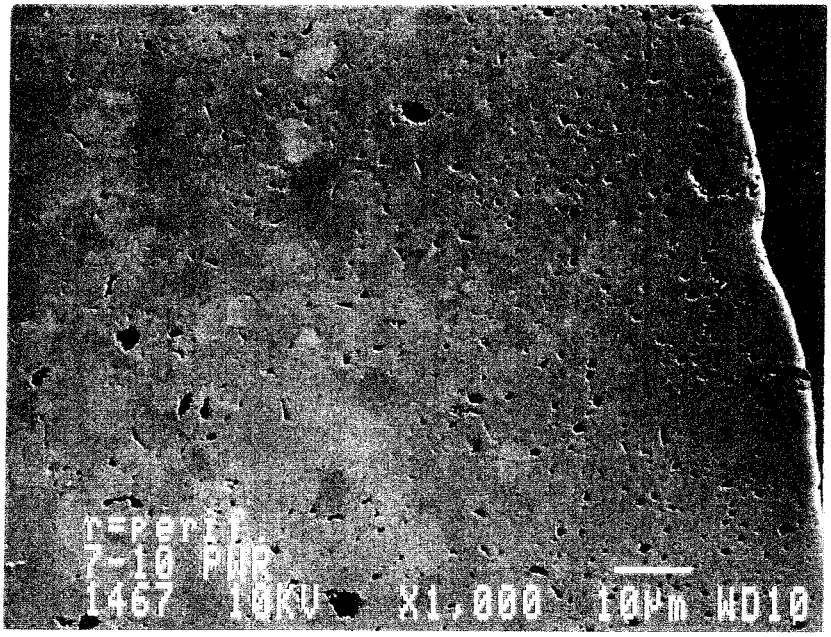

Figure 2-6. PWR reference fuel: (Burnup 43.0 MWd kgU)
Pellet rim zone. Polished surface (x 1000)

be fairly similar in width, about 30 - 40 microns, but an accurate estimation of the width is difficult, since the porous zones are poorly defined. Because of the poor definition, the value of the porosity at the rim in Figure 2-4 is of uncertain accuracy. In both fuels, the pores are of the order of 1 micron in diameter, and, in the judgement of the present author, are probably closed after reactor shutdown, and thus not readily available as corrodable surfaces. This, however, may not be true at higher rim burnups as the modification of the fuel microstructure becomes more extensive.
It will be shown later in this report (section 3.1) that there are other effects at the fuel pellet rim, enhanced burnup and alpha activity, which are dependent on the initial enrichment of the fuel, the neutron spectrum and the irradiation history. The formation of the porous zone at the pellet rim, however, appears to be mainly dependent on the burnup, and much work has been done in recent years to study the phenomenon and to establish the value of the burnup threshold.

In the SKB Spent Fuel Corrosion Programme, the lower segment rod 79B2, was selected as the spent fuel source for the Variable Burnup/Linear Heat Rating experiment, which had the aims of studying the effects on corrosion of **fuel structure**, and the corrosion behaviour of possible **fission product segregations**. The fuel burnup varied between 20 - 49 MWd/kgU along the pellet stack, and fuel cross-sections were selected at burnups of 21.2, 36.7 and 49.0 MWd/kgU for detailed characterization. The burnup values of the 3 specimens, and of intermediately placed corrosion test specimens, were established by means of burnup analysis by the Nd-148 method (16) of 2 specimens at the ends of the rod, and gamma spectrometric analysis of selected pellets (every third) along the stack. Figures 2-7 and 2-8 present SEM photomosaics of the rim zones of the 49.0 and 36.7 MWd/kgU specimens, and show both the polished and fracture surfaces.

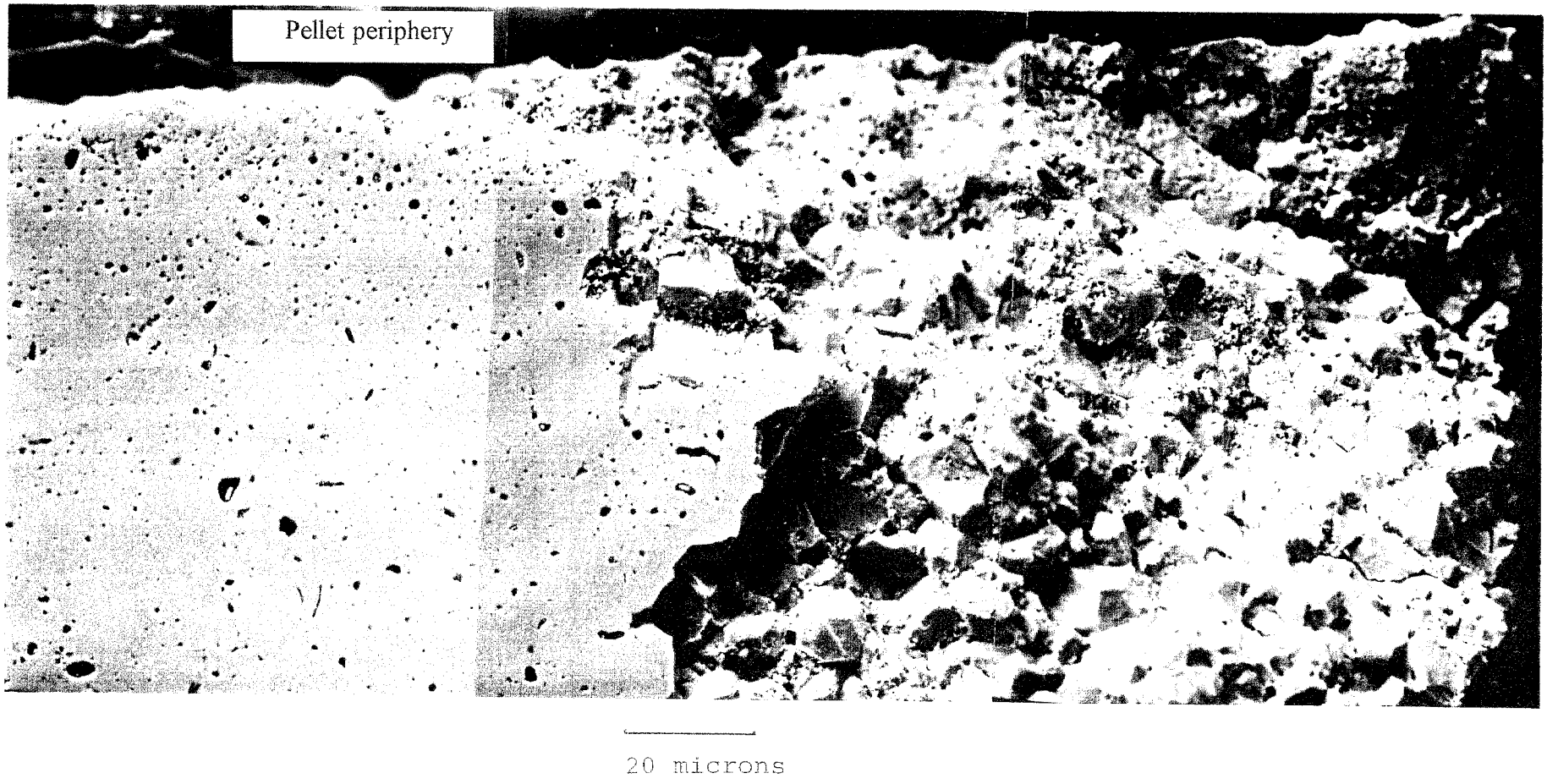

Figure 2-7. BWR fuel: (Burnup 49.0 MWd/kgU) Polished and fracture surfaces at the pellet rim. (x 1000)

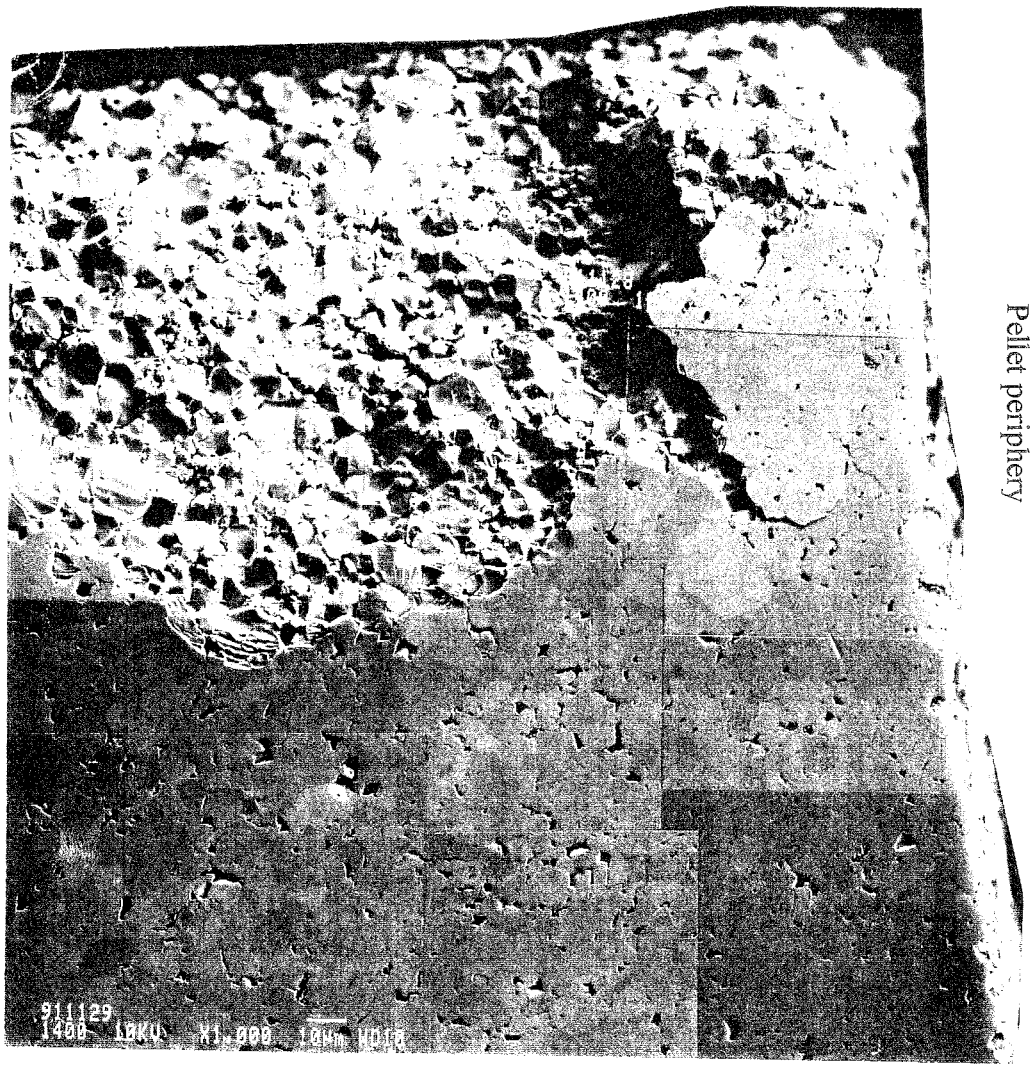

Figure 2-8. BWR fuel: (Burnup 36.7 MWd kgU) Polished and fracture surfaces at the pellet rim. (x 500)

Clearly, there is no porous zone at the rim of the 36.7 MWd/kgU specimen, and the fracture surface shows largely intragranular fracture, and no sign of the loss of definable grain structure which is seen in Figure 2-7. The porous zone visible at the rim of the 49.0 MWd/kgU specimen, however, is poorly defined, and only of the order of 20 microns wide, which is less than in the BWR and PWR reference fuels.

It should be pointed out here, that the SEM used in the Studsvik Hot Cell Laboratory is only radiation-shielded locally, and because of this, the size of radioactive fuel specimens is restricted to small specimens of dimensions about 10 x 1.5 x 0.2 mm in order to limit the radiation dose. Thus, only a small fraction of the pellet periphery (about 10%) can be examined on a particular sample, and if the rim effect is radially assymmetric, measurements of the width of the porous zone are associated with appreciable uncertainty. Such assymetric effects were observed by Barner et al (17) in a number of specimens included in the High Burnup Effects Program.

The High Burnup Effects Program was a large international group sponsered programme, organized and managed by Battelle Pacific Northwest Laboratories between 1978 and 1990. The main objective of the experimental programme was to study the effects of high burnup on fission gas release in LWR fuel. The programme included 82 fuel rods, of which 43, with pellet-average burnup levels ranging from 39 to 83 MWd/kgU, were subjected to post-irradiation examinations of relevance for this paper. It was noted that the width of the porous rim zone showed a correlation with the radial zone in which depletion of xenon had occured (See section 3.1), and the authors also developed an equation relating the zone width to the local burnup at the pellet rim:

$$w^2 = -21014 + 391.4\ (BU)$$

where w is the rim width in microns, and BU is the local burnup at the pellet rim in MWd/kgU. The rim burnup threshold for porous zone formation was thus 53.7 MWd/kgU. This equation, however, over-estimates the zone widths for the reference BWR and PWR fuels.

Walker et al (18,19), examined PWR fuel with average burnups ranging from 31.3 to 64 MWd/kgU, and concluded that the threshold average burnup for porous zone formation was 40-45 MWd/kgU, which is in good agreement with the SKB programme specimens. The authors also report that zone widths of 100-200 microns were observed in fuels of average burnups of 55-60 MWd/kgU, and, further, that in a specimen irradiated to an average burnup of 75 MWd/kgU in the Danish DR3 MTR, a heavy water reactor, the zone extended about 1.4 mm inwards from the rim (corresponding to 23% of the pellet radius). A similar large extension of the zone width has been reported by Kameyama et al. (20) in PWR fuel with an average burnup of 85 MWd/kgU.

Barner et al. (21) have recently revised their estimate for the threshold burnup for porous zone formation to a value of about 65 MWd/kgU at the pellet rim, which is in better agreement with the observations on the SKB reference fuels. (See section 3.1)

It is clear from the discussion above, that with current average discharge burnup levels of about 40 MWd/kgU, a significant fraction of Swedish spent fuel would be expected to show the formation of pellet rim zones displaying high porosity and modification of the fuel microstructure. As will be discussed in more detail later in this paper, the pellet rim is also associated with a higher local burnup and enhanced alpha and beta-gamma activity than in the bulk of the fuel pellet. Under the anoxic conditions expected in deep geological repositories, corrosion of spent fuel could occur either by dissolution of the $U(IV)O_2$ matrix or, if the radiolysis of water by alpha particles can sustain an oxidizing layer at the fuel surfaces, by oxidation to U(VI). Thus, the rim zone, with the combination of high porosity and local alpha dose rate, may be subject to preferential corrosive attack. Even a rim zone of only 50 micron's width represents almost 2% of the pellet volume, and 3-4% of the pellet fission product and actinide inventories. This is larger than the total amounts found in solution during semi-static corrosion tests over a period of

years, and since these are usually performed on relatively short-cooled fuel specimens, preferential attack could complicate evaluation of the test results.

However, the porosity at the rim is not the only microstructural feature of interest in this connection. It was mentioned above that the pellet rim is also associated with loss of definable grain structure in a process where the original fuel grains sub-divide into numerous smaller grains.

Figure 2-9 presents SEM photomicrographs of examples of the modified grain structure observed during the characterization of the BWR reference fuel, which, as mentioned above, had a high porosity zone of the order of 30-40 microns. The structure at the pellet periphery is shown in the micro-photograph at the left, while at the right, at higher magnification, an example of the grain subdivision process can be seen, at a distance of 100 microns from the periphery, thus extending further into the pellet than the porous zone. At this position, the new grains have a diameter of about 200 nm.

These observations prompted a more systematic SEM investigation of later specimens, and Figure 2-10 shows a SEM photomosaic of the fracture surface of the 49.0 MWd/kgU specimen from the 79B2 segmented rod. Figure 2-7 presented a SEM photomosaic at the same magnification of the pellet rim; Figure 2-10 shows a strip along the pellet radius at 90 degrees to that figure, and extends from the pellet periphery to about 230 microns into the pellet.
The figure also gives the radial positions of the sites of details of the modified grain structure which are presented in Figures 2-11 and 2-12. It can be seen that grain modification occured as far as 230 microns from the rim, which corresponds to a local burnup of about 53 MWd/kgU, appreciably lower than the burnup at the pellet rim, which was determined by electron probe microanalysis (EPMA) to be 66 MWd/kgU. (See Figure 3-7) The

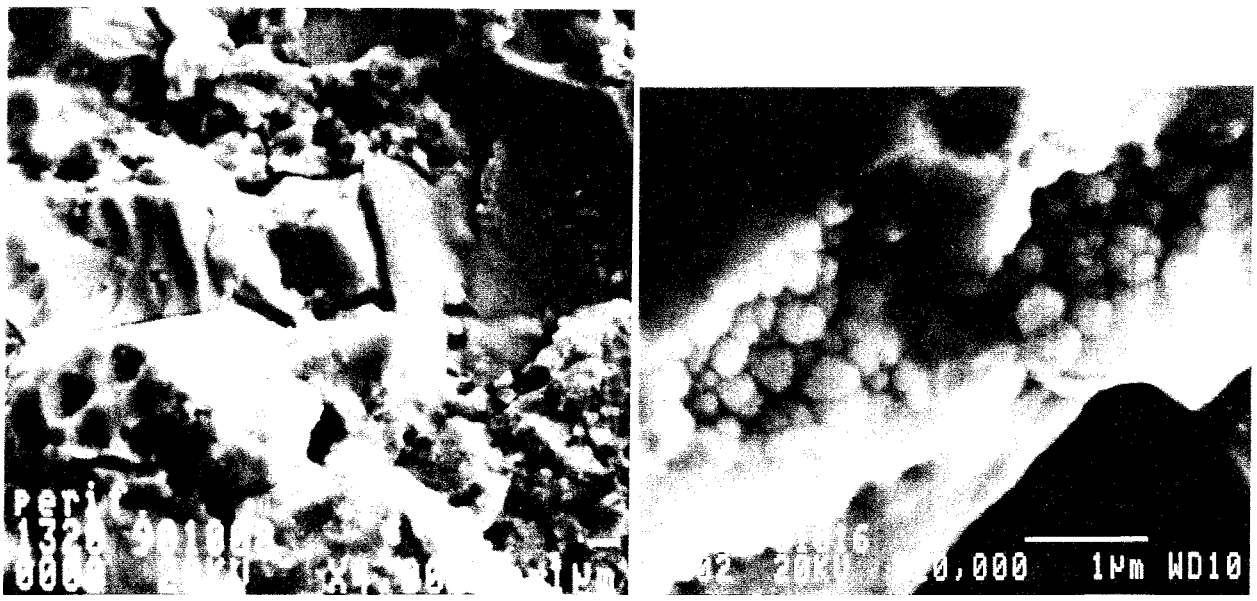

Figure 2-9. *BWR reference fuel; Recrystallized fuel grains: Left: at the pellet periphery (x 4000) Right: 100 microns from the periphery.(x 20000)*

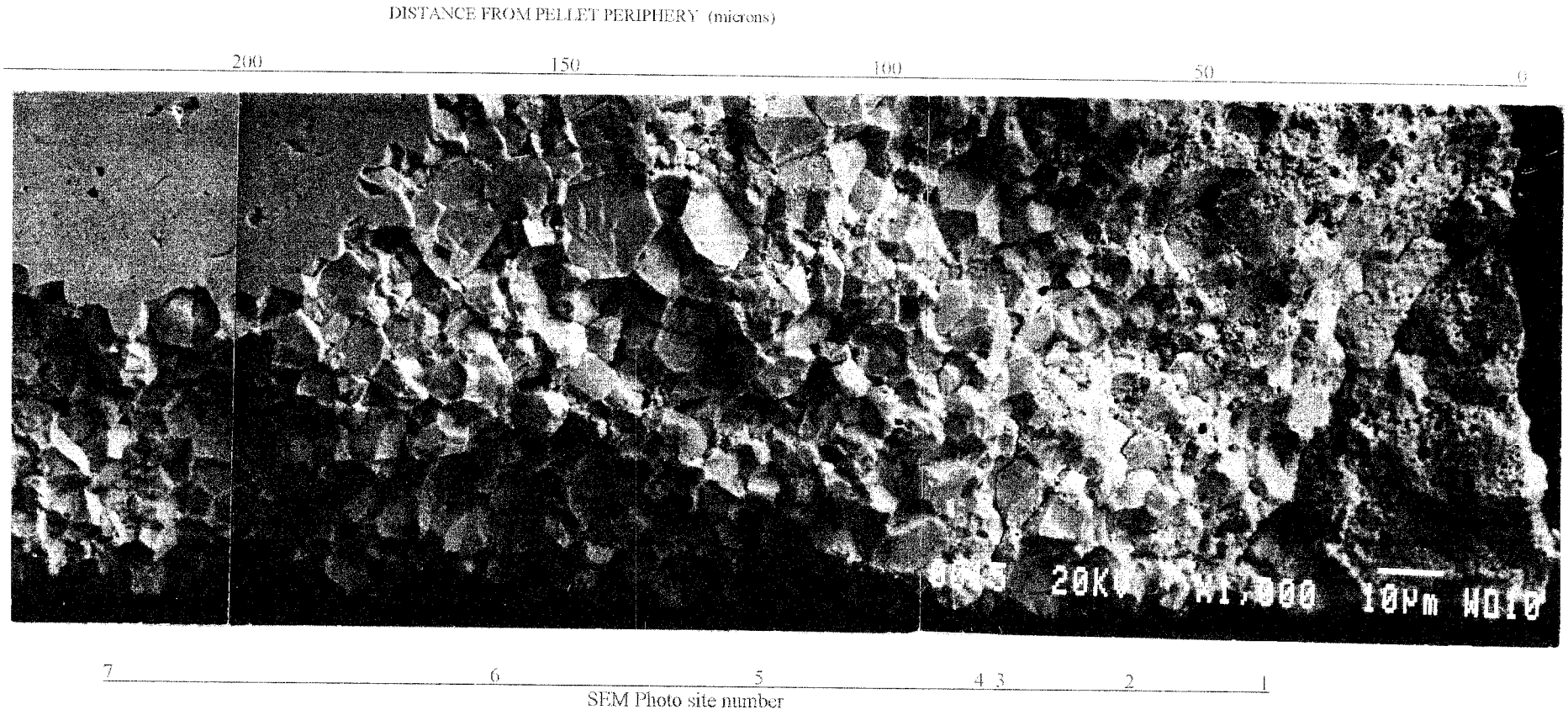

Figure 2-10. *BWR fuel: (burnup 49.0 MWd kgU) Fracture surface near the pellet rim. (x 1000) For detail of structure at the periphery and at sites 1-7, see figures 2-11 and 2-12.*

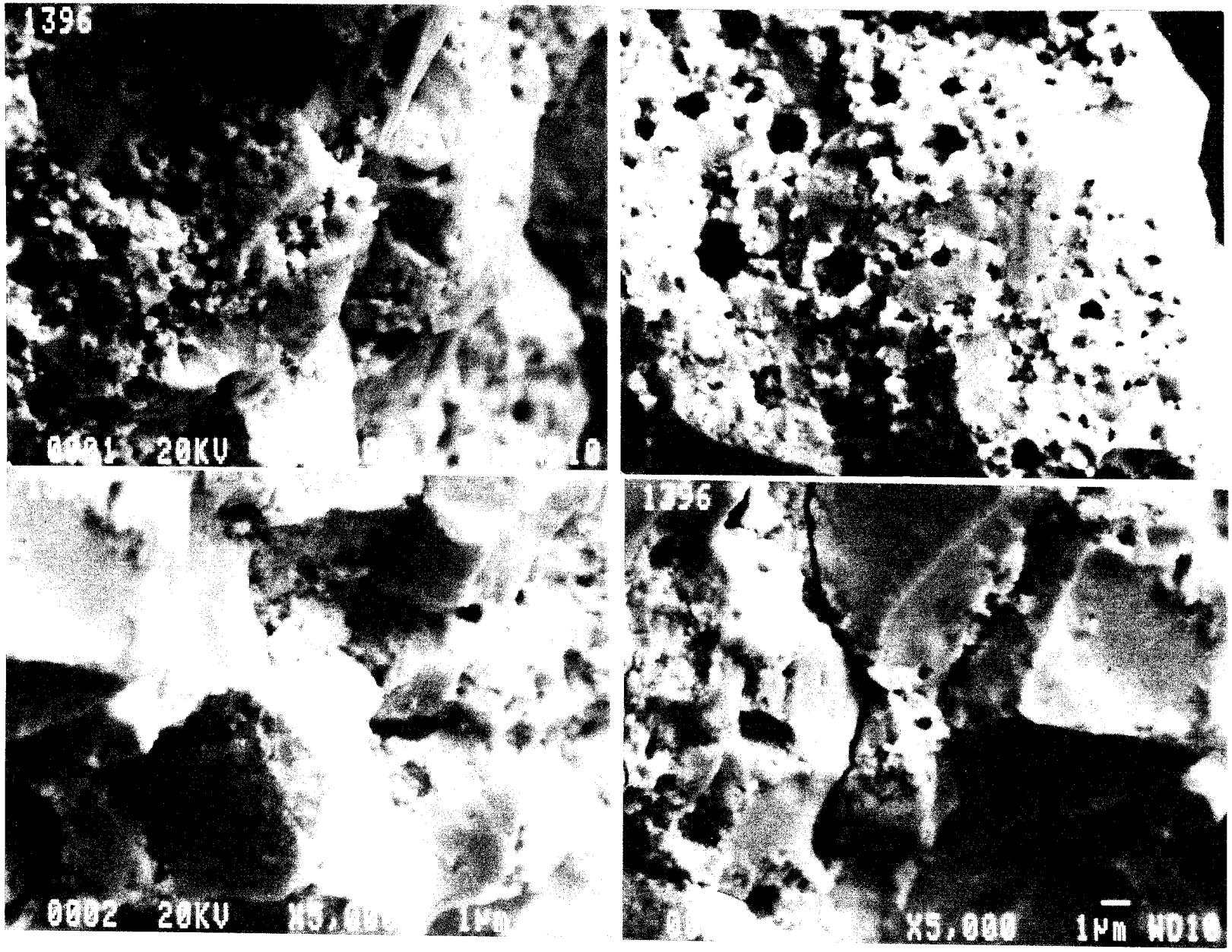

Figure 2-11. BWR fuel: (Burnup 49.0 MWd kgU) Detail of fracture surface (x 5000) At pellet periphery (top right) and at positions 1-3. (See Figure 2-10)

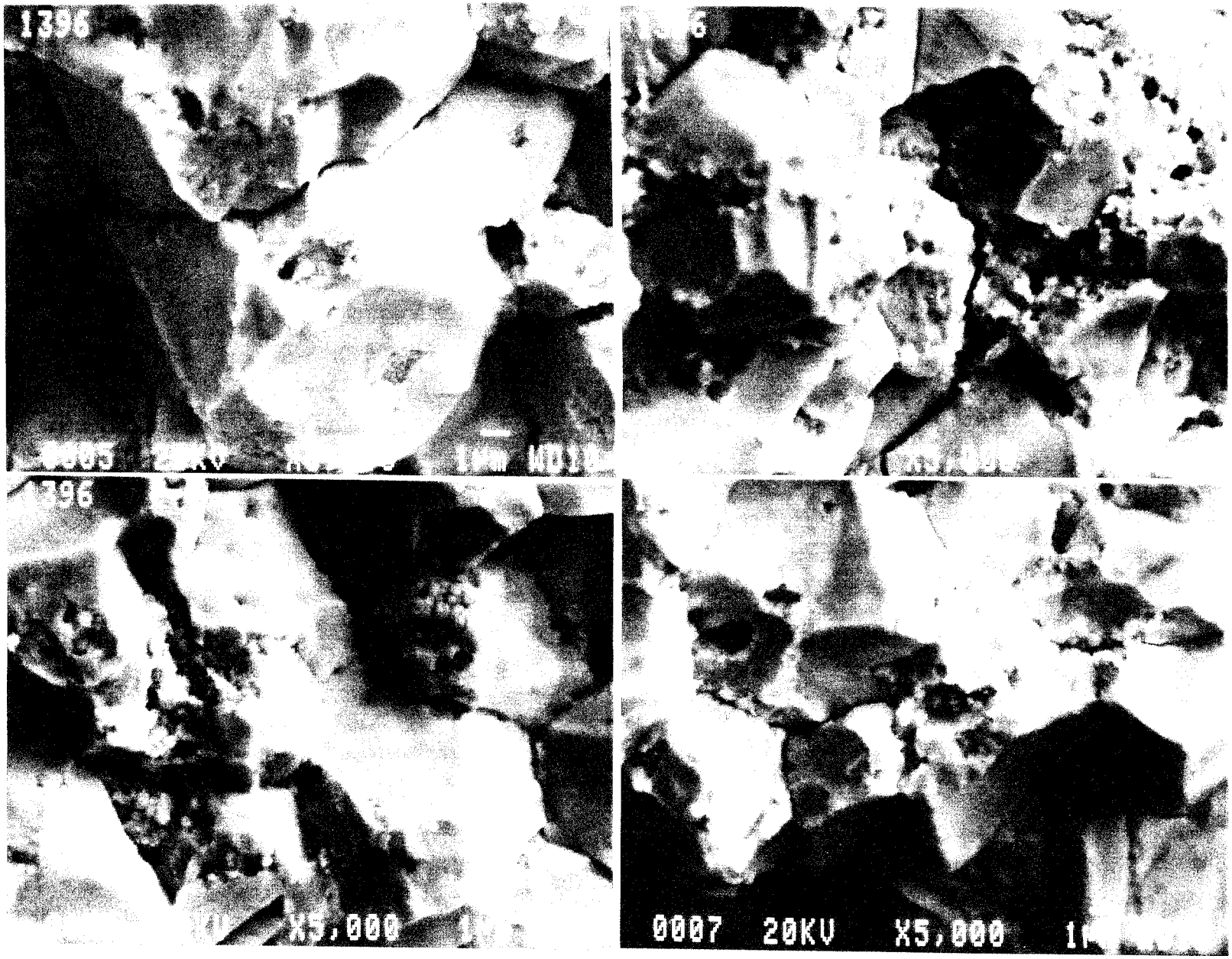

Figure 2-12. *BWR fuel: (Burnup 49.0 MWd/kgU) Detail of fracture surface (x 5000) at positions 4-7. (See Figure 2-10)*

width of the zone where grain subdivision occured was thus much larger than of the enhanced porosity zone, which for this specimen, was only of the order of 20 microns.
It can be seen that the modified grains often decorate pore surfaces, but also occur at grain edges and faces.

Photomicrographs of detail of the fuel fracture surface at 1.5 and 2.0 mm from the pellet rim, are presented in Figure 2-13 for comparison purposes, and show that, while traces of modified fuel grains persist far into the pellet, the effect is much diminished.

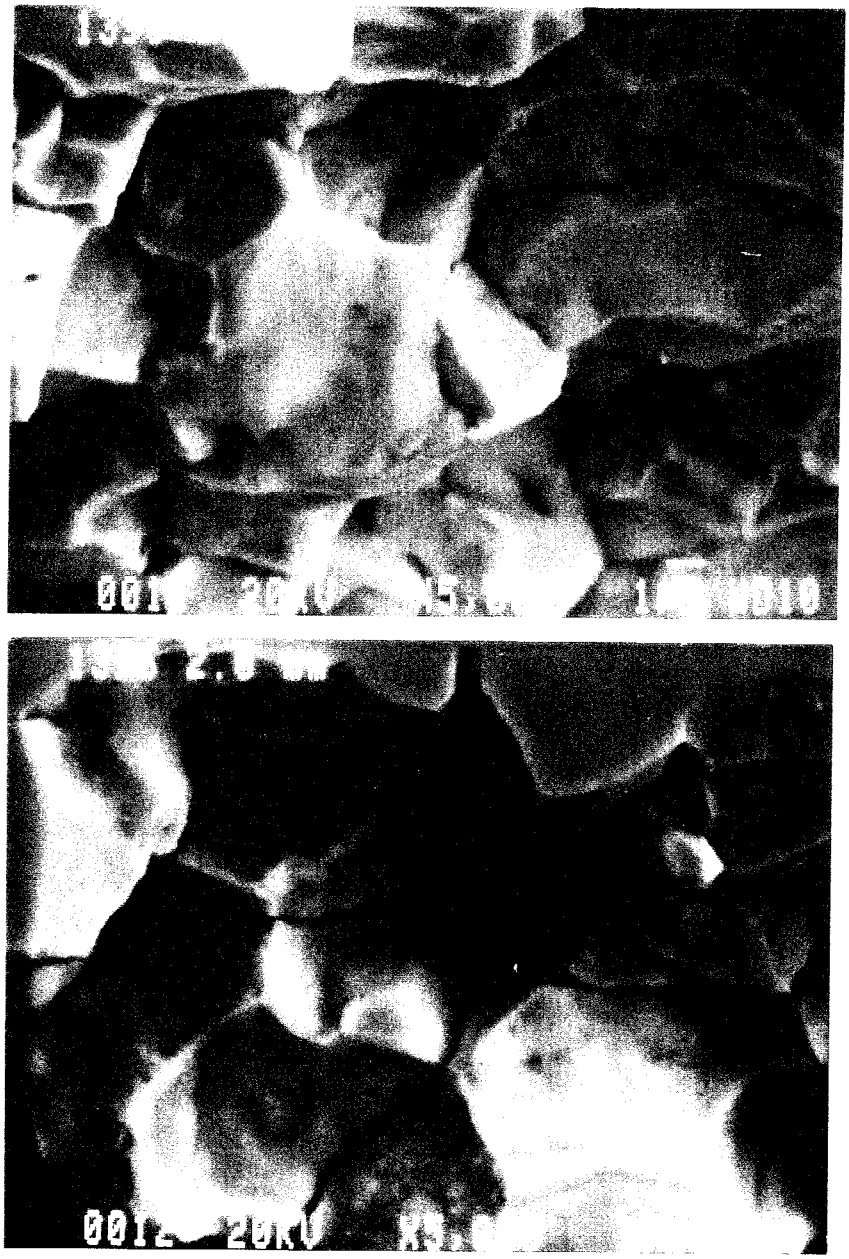

Figure 2-13. BWR fuel: (Burnup 49.0 MWd kgU)
Detail of the fracture surface at 1.5 mm (upper), and 2.0 mm (lower) from the pellet periphery. (x 5000)

Near the pellet centre, only sub-micron particles consisting of the 4d metals Mo, Tc, Ru, Rh and Pd are visible. (Figure 2-14)

With regard to the recrystallized fuel grains, the process for their formation, and its dependence on irradiation parameters such as local burnup and temperature are currently poorly understood. Their location at and near the pellet periphery, with higher fission product and actinide inventories, and higher fission fragment fluences, than in the bulk pellet, increased porosity, and the enhanced possibility of alpha radiolysis effects, may result in preferential corrosive attack, as was discussed above.

It has been suggested (22) that the grains consist of cesium uranates which are stable at the temperatures at or near the fuel pellet rim. However, even with the higher cesium fission product inventories at these positions, it is difficult to explain the extent of the subgrain formation. Also, EPMA-EDS examination of "colonies" of the grains in the 49.0 MWd/kgU fuel (23) gave spectra which were indistinguishable from the adjacent matrix.

Significant progress towards an understanding of the process for subgrain formation has, however, been made in recent years by Matzke (24,25), who has suggested that, in the rim zone, polygonization of the original fuel grains occurs by a cleavage process driven by small, high-pressure fission gas bubbles. Partial loss of the fission gases would be expected to be lost during the process, which is in qualitative agreement with the Xe concentration gradients observed experimentally in high burnup fuel by EPMA measurements.

In order to test the hypothesis, and to study the effects of dose and temperature on the process, Matzke and co-workers have performed simulation

Figure 2-14. *BWR fuel: (Burnup 49.0 MWd kgU) 4d metallic particles near the pellet centre. (x 5000)*

experiments in which single crystals of UO_2 were implanted with a range of doses of (usually) xenon, but iodine, rubidium and cesium beams have also been used. Shallow implants with 40 keV Xe ions were ineffective in producing polygonization, but with 300 keV ions at a dose of 5. 10^{16} ions/cm^2, SEM examination of the surface has shown a structure with some similarities to that seen at the rim of high burnup fuel (24). Interestingly, the dose mentioned above corresponds to a xenon atom concentration of about the same as that of **all** fission products in fuel with a burnup of about 70 MWd /kgU, that is, a value similar to the local burnup threshold for subgrain formation quoted earlier in this section.

The experimental programme consists of implantations at a range of temperatures (77 K, ambient and 773 K) and post-implantation anneals (400 C - 1500 C). The structural changes are followed by X-Ray Diffraction (XRD), Rutherford BackScattering (RBS), and Transmission and Scanning Electron Microscopy (TEM, SEM).

Clearly, the presently available results of the programme show great promise of further definition of the mechanism for subgrain formation, and quantification of the required parameters of dose (burnup) and temperature.

3. ACTINIDE AND FISSION PRODUCT DISTRIBUTIONS

3.1 FORMATION

The local fission rates of U-235 by thermal neutrons over the cross section of a fuel pellet are subject to radial and angular assymmetries due to effects such as flux depression by self-shielding, position in the assembly, and proximity to control rods etc., and, of course, are also dependent on the irradiation history and burnup.

However, of most potential relevance for the corrosion of spent fuel in groundwaters is the formation and fission of plutonium isotopes, and the build-up of other actinides, at the pellet rim due to resonance capture of neutrons in the epithermal energy range. The resultant steep gradients of both burnup and alpha activity in this zone have been mentioned several times in the discussion above of the fuel structure at and near the fuel pellet periphery.

In Figure 3-1 are shown alpha and beta-gamma autoradiographs of a transverse cross-section of the PWR reference fuel, performed as routine parts of the post-irradiation examination of this fuel (2, 8). Since this fuel, fairly typical of most spent fuel, had experienced only "normal" linear heat ratings and temperatures during its irradiation, and, hence, little or no fission product migration or segregation had occured, the beta-gamma autoradiograph is fairly featureless, showing only the fuel cracks due to activity channeling.

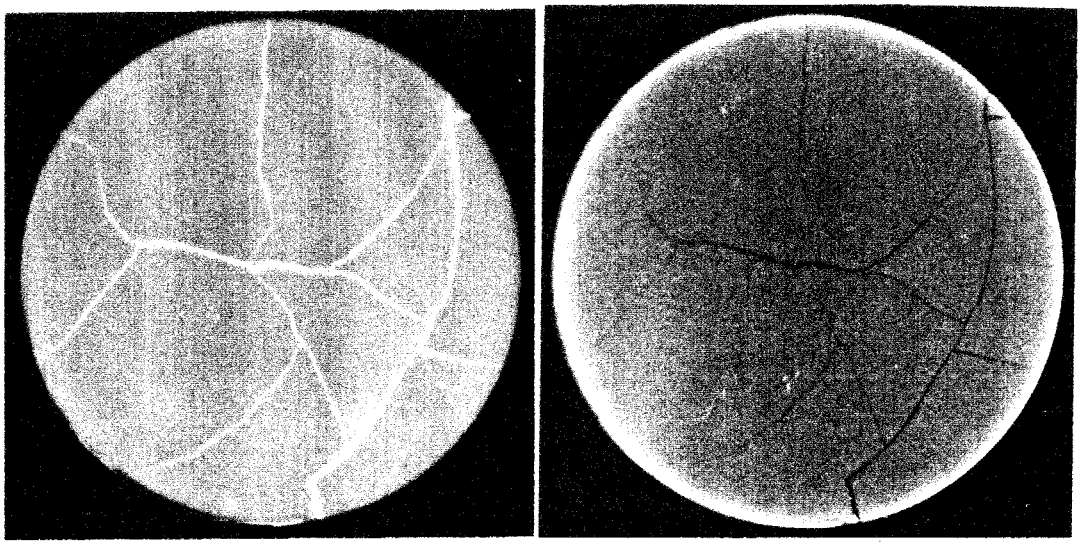

Figure 3-1. *PWR reference fuel: (Burnup 43.0 MWd/kgU) Autoradiographs of fuel transverse section. (x 7.4) Beta-gamma: (left) Alpha: showing rim effect (right).*

There is no evidence of a fission product (burnup) gradient because of the "smearing" of the exposure by the relatively long-range beta particles and gamma photons.

The alpha autoradiograph, on the other hand, clearly shows the higher rim concentration of alpha-emitting actinides. Attempts to quantitatively measure the alpha concentration gradient by optically counting the etch pits in the autoradiographic film have been made previously (26), but the method is both tedious and inaccurate, since precise definition of the pellet edge is difficult due to the short exposures which are required. Another method for quantitative measurement of the gradient will be described below.

Diametral gamma scanning of slices of spent fuel can give some information on the burnup gradient, although even here the method is limited by poor radial definition due to collimator size. Figure 3-2 shows the results of scans over the PWR fuel slice examined in Figure 3-1. The measurements were performed (2) using a 1 x 2 mm collimator, with steps of 0.1 mm at the rim,

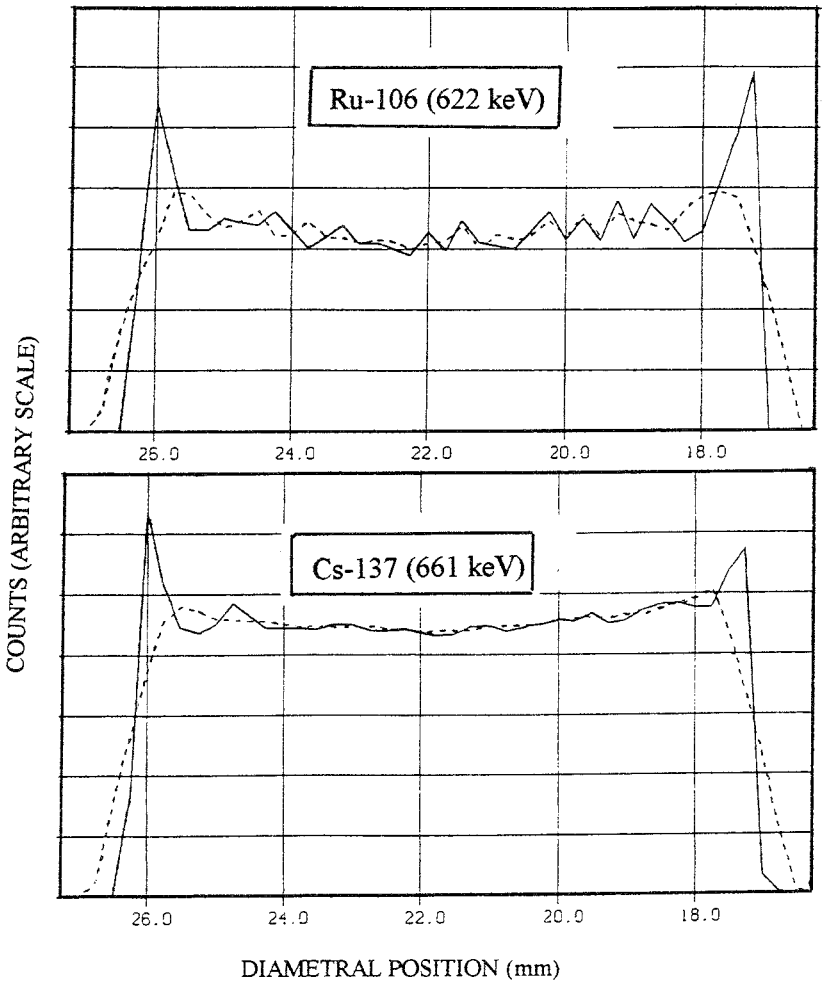

Figure 3-2. *PWR reference fuel: (Burnup 43.0 MWd/kgU). Diametral gamma scan of transverse section showing rim effects for Cs-137 and Ru-106, but with enhancement of the latter due to fissions in Pu.*
(Solid line: measurement points corrected by one-dimensional tomography)

and 0.25 mm over the rest of the diameter. Full details of the measurement and correction procedures are given in the reference. The figure shows the uncorrected and corrected (solid lines) results for Ru-106 and Cs-137.

Both nuclides show enhancement at the pellet rim, but it can also be seen that the Ru-106 enhancement is larger than that for Cs-137. This is a reflection of the larger fraction of fissions of Pu-239 at the rim than in the bulk pellet, since the fission yield of Ru-106 is an order of magnitude higher in Pu-239 fission than in U-235. As will be discussed later, this fission yield shift (in the lower mass fission yield peak) has consequences for the inventaries of fission products, and, possibly, for the fuel stoichiometry.

The burnup profiles of the reference fuels used in the SKB Spent Fuel Corrosion Programme have been determined by Electron Probe Micro Analysis (EPMA) on polished specimens of the fuels (23). The measurement procedures were essentially the same as those employed in earlier work (27).

For the BWR and PWR reference fuels, the measured Nd/U ratios from selected radial positions, with close spacing over the rim zone, were corrected to local burnup at each position, and then the smoothed curve of the profile was used for a radially-weighted normalization to the burnup of the bulk pellet (in a closely located pellet) as determined by destructive analysis (16). In the case of the specimens with burnup 21.2 and 36.7 MWd/kgU from the BWR segment rod used for the Variable Burnup/Linear Heat Rating Experiment, normalization was performed to bulk pellet burnups calculated by interpolation between the measured burnups of the destructively-analyzed pellets.

The measurement of **the alpha activity profiles** of the fuels was performed by the photodensitometric scanning of alpha autoradiographs taken on polished whole cross-sections (28). In the method employed, the specimens are mechanically pressed against the film in order to ensure a hard and even contact, so the autoradiographs usually showed good definition.The 5 specimens, the BWR and PWR reference fuels and the 3 fuels of different burnup from the 79B2 segment rod, were examined in two independent campaigns. All the exposed films in a particular campaign were etch-developed under the same conditions.

Since film darkening is non-linear, and the range of intensities was very large, a photodensity calibration curve was constructed in a separate campaign using a sixth fuel specimen, the reference fuel from an experiment performed to study fission product migration and leaching (29). This specimen, which had a shorter cooling time than the others in the programme, had the highest alpha activity, and by performing a series of ten exposures of between 5 and 50 seconds in 5 second steps, a wide range of film photodensities was produced.

The autoradiographs were scanned over the pellet diameter in a photodensitometer at low speed (40 microns/second) with a 30 x 30 micron collimator. The linear scaling factor was 50, which produced scans which could be eval-

uated manually. The ten calibration scans were smoothed, and the photodensities measured at frequent intervals along the pellet diameter, with a larger frequency at the rim positions, which were most subject to non-linearity errors. The resultant calibration curve was later applied, point by point, to the scans of the other 5 specimens, which were scanned in the same way.

Having, thus, established the relative alpha activity profiles of all the six fuel specimens, corrected for the non-linearity of photodensity, absolute calibration was effected by means of the results of the destructive analysis of the fuel specimens used for inventory determination, as was described above for the burnup profiles. Here, the results of alpha spectrometric and Inductively Coupled Plasma-Mass Spectrometric (ICP-MS) analysis of solutions of the bulk pellets were used. Again, as in the case of the burnup profiles, the alpha activity profiles were radially-weighted before comparison with the bulk pellet results. The 21.2 MWd/kgU burnup specimen from the BWR segment rod was excluded from the calculation of the mean absolute calibration factor, partly because of the low photodensity, but mainly because of uncertainty in the calculation of the specimen inventories. The average of the calibration factors (photodensity/second exposure to Bq/g Uranium) of the other five specimens showed only a 8% standard deviation.

The burnup and alpha activity profiles for the PWR reference fuel, measured and corrected as described above, are presented in Figure 3-3, and the alpha autoradiograph (longitudinal cross-section) and burnup and alpha activity profiles for the BWR reference fuel in Figures 3-4 and 3-5 respectively.

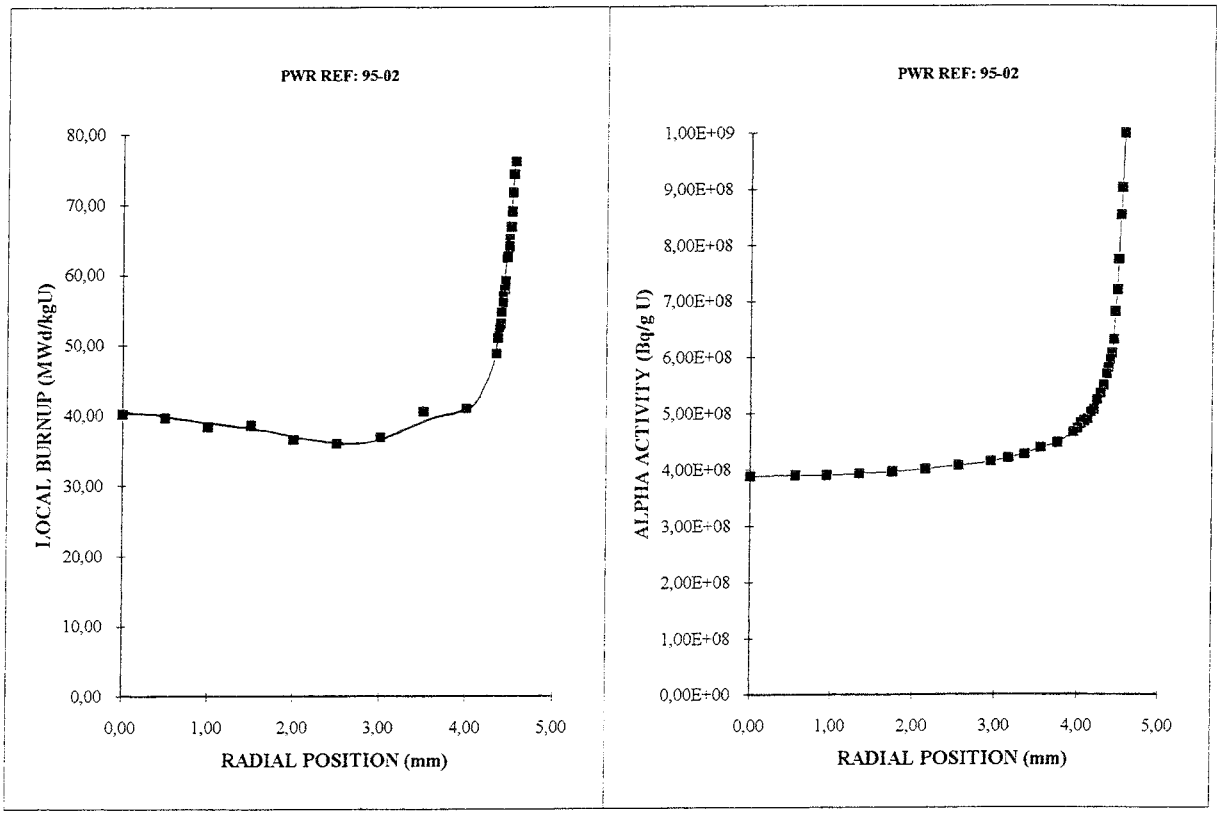

Figure 3-3. *PWR reference fuel: (Burnup 43.0 MWd/kgU) Local burnup and alpha activity as a function of radial position.*

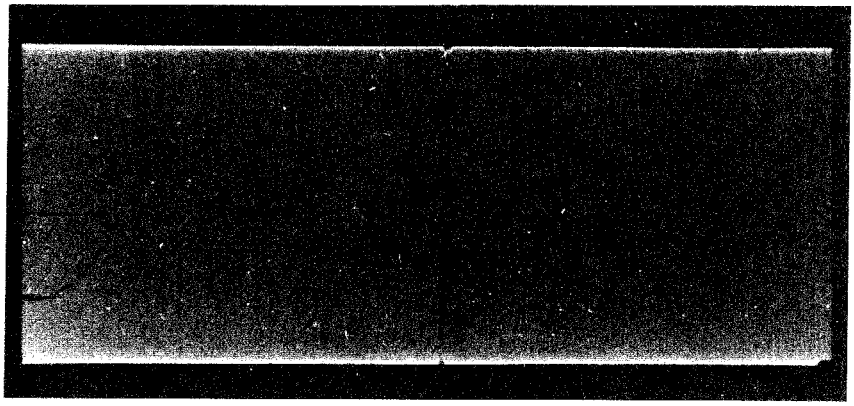

Figure 3-4. *BWR reference fuel: (Burnup 42.0 MWd kgU) Alpha autoradiograph of longitudinal cross-section. (x 4)*

From Figures 3-3 and 3-5, it can be seen that the burnup and alpha activity profiles for these two fuels, which had almost the same burnup and decay times, are very similar. The PWR fuel, however, appears to have a higher rim burnup than the BWR fuel, although this is at least partly due to the effect of the apparent minimum in the burnup profile between radius 2 - 3 mm., which caused an increase in the calculated rim burnup during the radial-weighting process. Each point in the burnup curve is the mean of 5 measurements; the standard deviations of these 3 points were similar to the others in the figure, so the apparent minimum is both unexpected and unexplained.

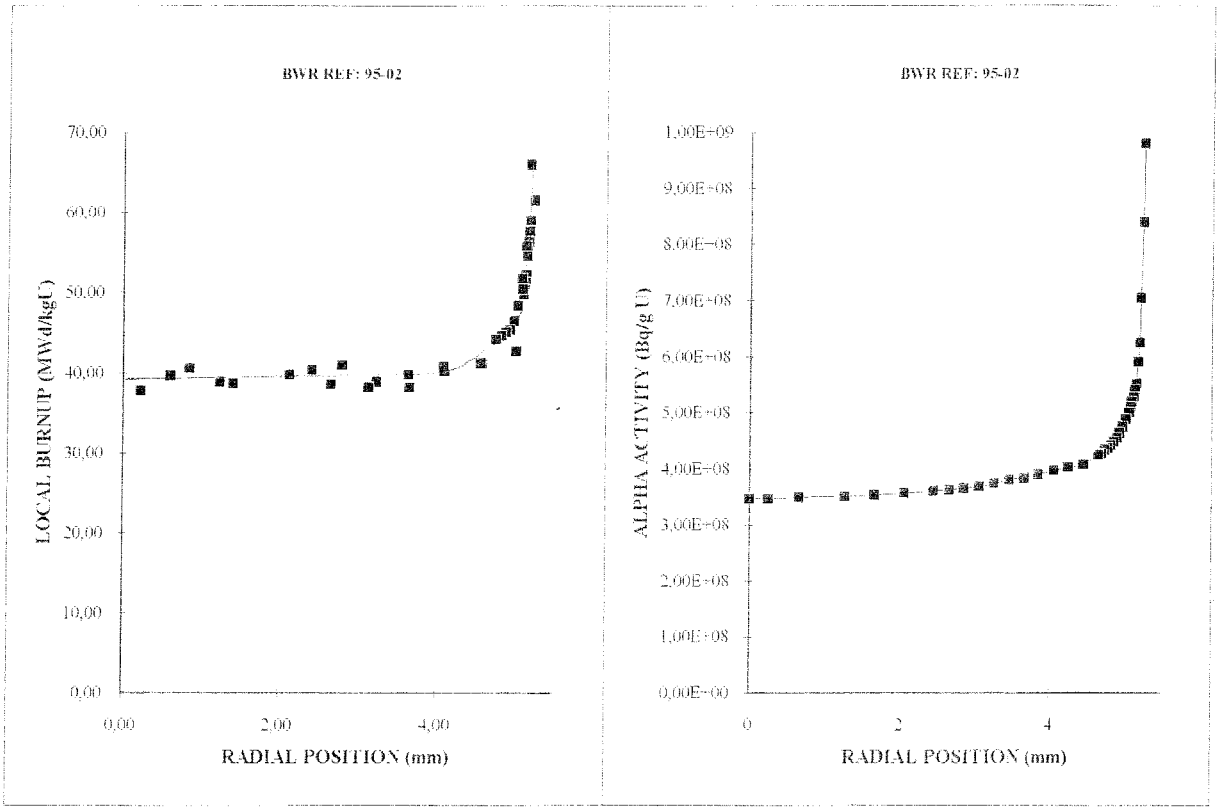

Figure 3-5. *BWR reference fuel: (Burnup 42.0 MWd kgU). Radial variation of local burnup and alpha activity.*

The local burnup values from these figures, however, have been used earlier in this report during the discussion on fuel structural effects at and near the pellet rim.

With regard to the alpha activity profiles, it can be noted here that the measurement technique should be considered only semi-quantitative. Apart from inaccuracies due to signal noise, and definition of the rim position, (the 30 x 30 micron collimator aperture is large relative to the width of the rim zone), there are uncertainties regarding the response of the autoradiographic film to different alpha particle energies at these exposures. Although the relative actinide compositions vary over the pellet diameter, and particularly so over the steep gradient at the pellet rim, the method equates film darkening with particle numbers rather than deposited energy. In spite of this, the good agreement between the results of the absolute calibration procedure suggests an accuracy of about +/- 15%.

These observations are particularly relevant with respect to the characterization of the 3 ceramographic specimens from the 79B2 BWR segment rod. 16 other fuel/clad sections from the rod, with average burnups ranging from 27.0 to 48.8 MWd/kgU, are currently being subjected to corrosion testing in a bicarbonate groundwater under oxic and anoxic conditions. (See reference 30 for a description of the experiment, and some early results.) One of the main aims of the experiment is the study of the effects of spent fuel structure on the corrosion mechanism(s). The specimens have to date been exposed for about 5 years to a series of static contact periods with the groundwaters, solution concentrations of selected nuclides being determined after each contact by conventional radiometric and radiochemical analysis, and also by ICP-MS analysis. On completion of the experiment, the specimens will be subjected to a detailed post-irradiation examination in an attempt to identify possible corrosion products and sites of preferential corrosion.

Detailed and systematic SEM characterizations have been performed of the fuel structure of the 3 ceramographic specimens, which have burnups which span the range of the corrosion test specimens. As shown above, the corrosion test specimens with burnups higher than about 40 MWd/kgU, may have developed structural pellet rim zones during irradiation, while along the pellet stack, the burnup gradient would be expected to have produced a steeper axial gradient of pellet actinide contents, associated with radial gradients in each fuel pellet. However, since the concentration ratios of the actinides will also vary axially and radially, comparison of the absolute values of local alpha activity determined by the autoradiographic method will be subject to greater uncertainty than when the BWR and PWR reference fuels are compared. Fortunately, the differences are so large that the error is probably negligible.

Photomacrographs and alpha autoradiographs of the 3 specimens are shown in Figure 3-6, and the radial burnup and alpha activity profiles in Figure 3-7. All three autoradiographs were performed with the same exposure time in order to demonstrate qualitatively the large increase in alpha activity with increased burnup, but it is expected that the report copies will be less illustrat-

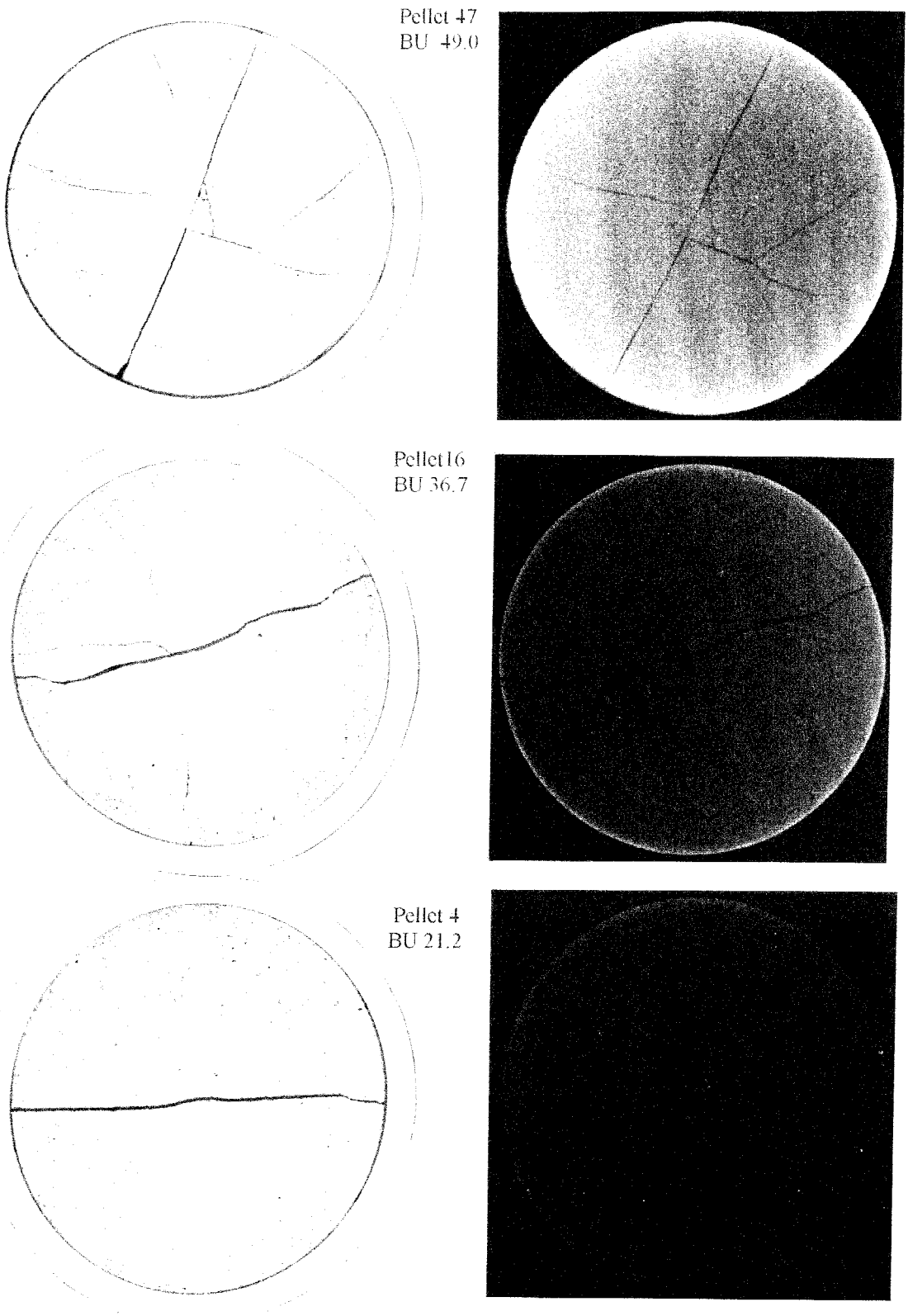

Figure 3-6. *BWR segment rod 79B2. Photomacrographs and autoradiographs of fuel of different burnups (x 6)*

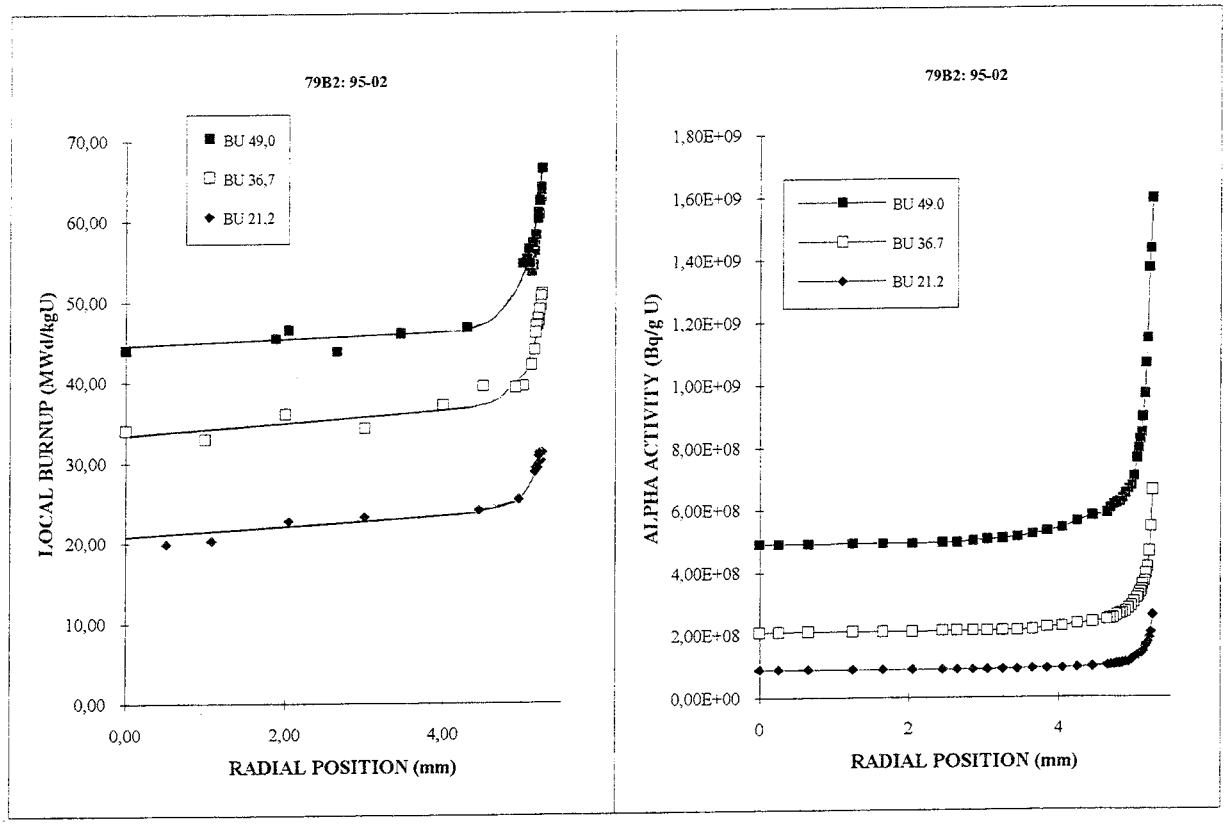

Figure 3-7. *BWR segment rod 79B2: Radial variation of burnup and alpha activity for fuel of different burnups.*

ive of the effect than the originals. The effect, however, is clearly seen in Figure 3-7. Although the local burnup along the fuel pellet stack, i.e., including the pellet rims, varied by a factor of about 3.5, the corresponding variation in the local alpha activity was by a factor of about 15. The significance of these observations for the corrosion of spent nuclear fuels in groundwaters will be discussed later in this section.

First, however, it is necessary to consider the different time dependencies of the burnup and alpha activity profile results. While the local burnup itself, of course, is independent of decay time, the inventories and activities of the fission products after reactor shut-down are determined by the local fractions of fission events in uranium and plutonium isotopes. Although, as mentioned above, there are significant differences in the fission yields of a number of nuclides between the fissile species, these are well-known, and calculation of the inventories can be performed with satisfactory accuracy by available codes.

Calculation of actinide inventories and their variation with time, particularly at the pellet rim, is associated with greater uncertainty because of the more complicated problems of definition of the neutron spectrum and the rates of neutron absorption reactions. For example, in the case of the 79B2 BWR lower segment rod discussed above, the long and complicated irradiation history, control rod movements and the effect of void fractions, may advers-

ely affect the accuracy of calculation. Further, after reactor shut-down, the actinide inventories are more subject to variations due to decay-growth relationships than those of the fission products, the most noteworthy of these being the growth of Am-241 by decay of Pu-241.

For the long-term corrosion of spent fuel,of course, it is the long-lived Pu isotopes and Np-237, which dominate the actinide inventories, and represent the potential cause of alpha radiolysis effects. The alpha activity of the spent fuel used in corrosion tests designed to identify corrosion mechanisms, and to establish their rates, however, mostly consists of actinides with relatively short half-lives, particularly at the pellet rim. It is, therefore, important to have a good understanding of the the composition of the local alpha activity and its variation with time in order to be able to evaluate corrosion test results and apply them to a model of long-term corrosion. It will be clear from the discussion above, that, at a given decay time, the alpha activity and its radial distribution in the fuel, will be extremely dependent on initial fuel parameters and on the irradiation history. Further, experimental validation of code calculation results is difficult because of limitations in sampling and analytical techniques.

Garcia Alonso et al. (31), however, have performed such measurements on a PWR pellet with an average burnup of 55 MWd/kgU. In Figure 3-8 are shown radial profiles of selected nuclides, which have been replotted from the figures in the original paper.

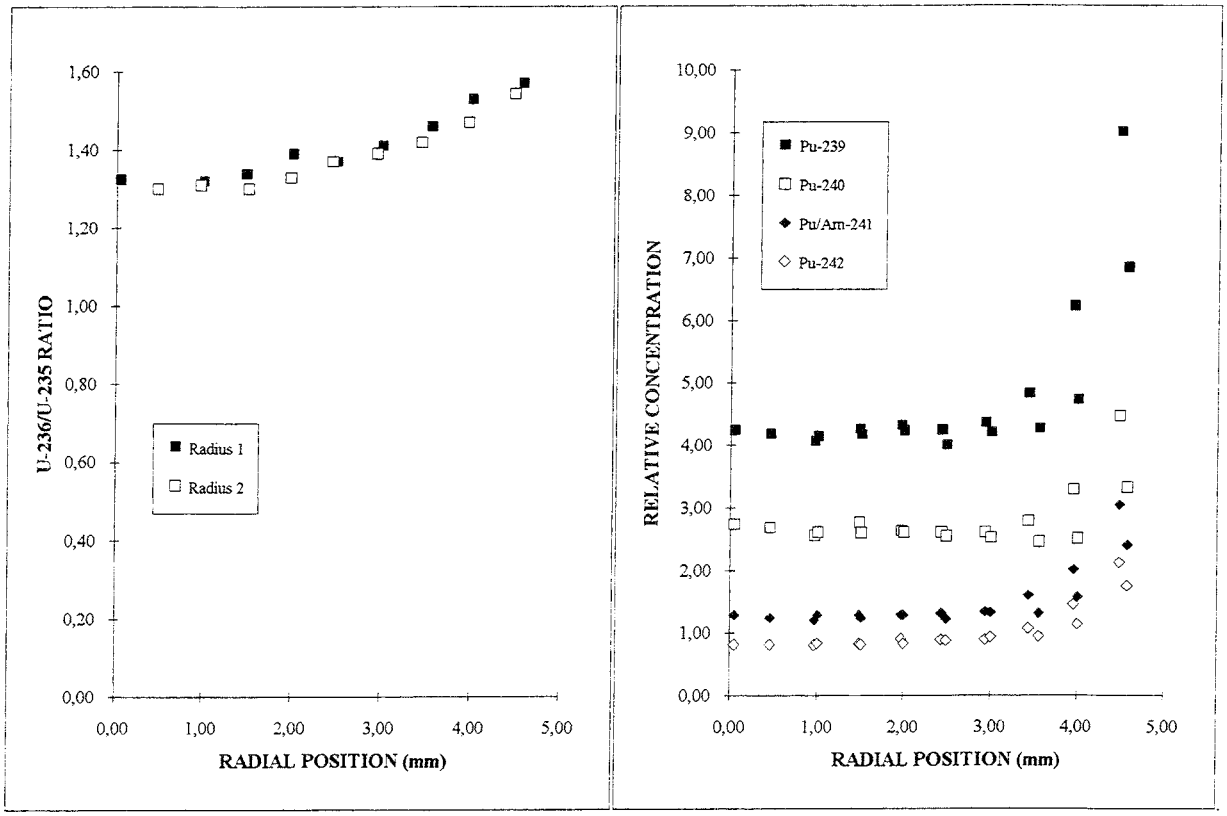

Figure 3-8. *Radial variation of the U-236/U-235 ratio, and the concentrations of Pu isotopes determined by laser ablation and ICP-MS. (Replotted data from the paper by Garcia Alonso et al. Reference 31.)*

The authors coupled sample-taking by means of laser ablation of the pellet surface (stepwise along 2 radii) with analysis by ICP-MS. Both selected fission products and actinides were analyzed. As is pointed out in the original paper, spatial resolution is poor, since the laser-formed crater which is sampled had a diameter of about 500 microns, which is large compared with the pellet rim zone, so that the Pu concentration results at the actual rim are probably underestimated. In spite of this, a large upswing is observed for all the 4 isotopes plotted.

The figure also shows the radial variation of the U-236/U-235 ratio.There is a decrease in total uranium concentration at the pellet rim which can be measured by the EPMA technique (23). Also over the rim zone, although most of the fission events occur in Pu isotopes, some fissions occur in U-235, while the U-236 content stays about constant, thus giving an increased ratio between these isotopes as the rim is approached.

This effect has been used in a tentative attempt (32,33) to detect possible preferential corrosive attack at the rims of fuel specimens from the 79B2 BWR rod, by comparing values of the ratio determined by ICP-MS analysis of corrosion test solutions with values calculated for the bulk fuel and rim. The ratio values for the bulk fuel were normalized to the ICP-MS results on the inventory specimens. (See above). Although the calculation of the ratios at the pellet rims was much simplified (being based on an extensive series of ORIGEN calculations), the results suggested that corrosion of these specimens appeared to be of the bulk pellet, rather than by selective attack at the pellet rim. These studies are continuing with all the reference fuels and corrosion test solutions, but emphasis is also being placed on experimental determination of the U-236/U-235 ratios in the fuel, and on code validation.

Another approach to the problem of the determination of the individual actinide profiles has recently been examined (34). From the fuel from a 20 mm long segment of the BWR reference rod, 8 small fuel particles were selected at random, and 2 further specimens were taken by scraping the periphery of one of the larger (> 4 mm) fuel fragments. These specimens were dissolved in HNO_3, and then analyzed for actinide contents by an ICP-MS method developed for the analysis of corrosion test solutions (35). Dilutions of these solutions were also examined by alpha spectrometry and analyzed for uranium contents by laser fluorescence. Uranium concentrations in the original solutions were at about the 2000 ppb level.

By ICP-MS analysis, all mass peaks over the range 235-244 were measured, and the concentration ratios of the transuranium nuclides to total uranium were calculated. The 241 peak consisted of both Pu-241 and Am-241. Since the radial positions of the 8 randomly selected particles were unknown, the ratios were plotted against the U-236/U-235 ratios. (See discussion above). Typical results of "high" (Pu-239) and "low" (Cm-244) abundance nuclides are shown in Figure 3-9, which shows appreciable scatter in the results, but the rim profiles are defined with reasonable accuracy. Figure 3-10 presents the nuclide profiles where the nuclide /uranium ratios have been normalized to the mean of the 3 specimens with lowest U-236/U-235 ratios.

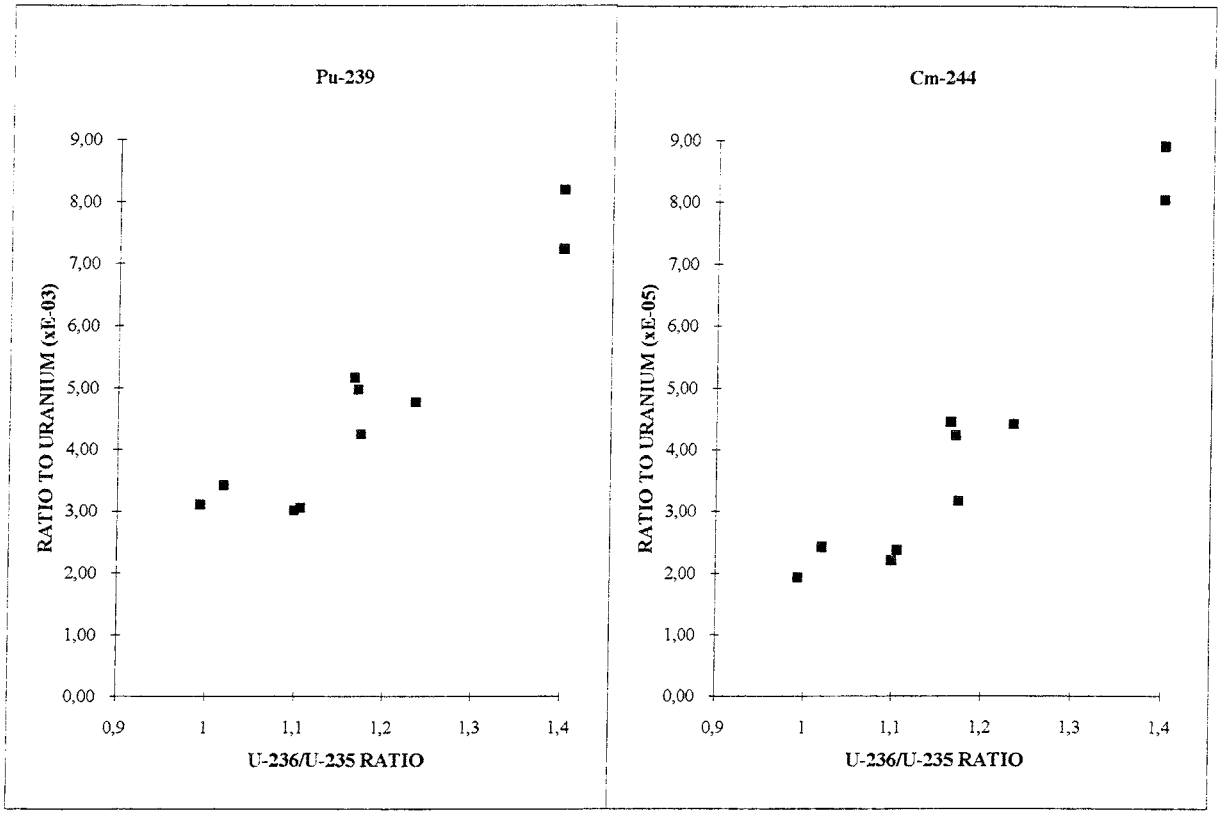

Figure 3-9. *BWR reference fuel: Relative concentrations of Pu-239 and Cm-244 in randomly selected fuel particles versus U-236/U-235 ratio.*

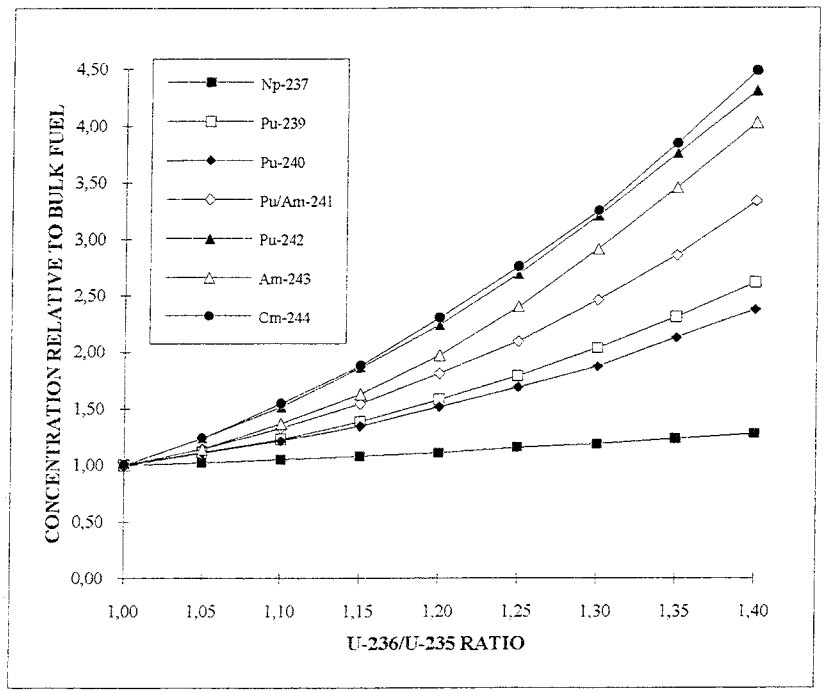

Figure 3-10. *BWR reference fuel: Radial variation (non-linear) of normalized actinide concentrations.*

These mean values showed good agreement with the values obtained on the inventory specimen, and therefore correspond to the bulk pellet average. Thus, the normalized profiles plotted in Figure 3-10, represent radial positions from about radius 4.75 mm out to the pellet rim (Compare with Figure 3-5), but are non-linear with respect to radius.

Inspection of Figure 3-10 shows that, as would be expected with the combination of fission and multiple neutron capture reactions at the pellet rim, the profiles are steeper for the higher mass nuclides. At the time the autoradiography was performed on this fuel specimen (December 1991), it can be seen from Figure 3-5 that the total alpha activity at the pellet rim was about 1. E 09 Bq/g U. From the analytical results on the fuel particles, which will not be presented in detail here because of space considerations, it can be estimated that, of this activity, about 92% was from Pu-238, Am-241 and Cm-244, (19, 26 and 47% respectively), and only about 8% from long-lived nuclides.

For this specimen, even after a total storage time of 30 years, the rim alpha activity can be calculated to decrease by only about 10%, since the decay of the shorter half-life nuclides Pu-238 and Cm-244, is largely compensated by in-growth of Am-241. Although the alpha profiles and nuclide compositions for spent fuel with different burnups and irradiation histories will show large variations, this will be generally the case for all specimens of average burnup of 40-50 MWd/kgU.

Thus, over the period of time when, hopefully, all corrosion tests on spent fuel are performed, the **potential** for alpha-radiolysis induced corrosion will be larger at the pellet rim than in the bulk fuel, if only the local alpha activity levels are considered. The locally-deposited **alpha dose** to ingressed water, however, will be determined by the distribution and magnitude of free volume (cracks, residual pellet/clad gap) in the fuel rod, and the microstructure of the fuel. As mentioned above, the high porosity rim zone is of great interest in this respect, particularly the question of whether the porosity is open or closed, and much current research work is being directed its study, by means of both fuel characterization (pre- and post-corrosion) and the evaluation of the corrosion tests themselves.

3.2 FUEL STOICHIOMETRY

At the beginning of section 3.1, it was mentioned that with increasing average burnup, the fraction of fissions in Pu-239 increases in the bulk of the fuel pellet, but more particularly at the pellet rim. This results in a shift in the lower mass peak in the fission yield spectrum, which changes the relative concentrations of the chemical elements in the accumulating fission product inventories. In particular, there is a significant increase in the yields of the elements which are the main components of the 4d metal particles (Mo, Tc, Ru, Rh and Pd, of which the latter three are noble metals).

The possibility that these changes could lead to changes in the oxide stoichiometry, and, therefore to changes in properties such as thermal conductivity and fission gas release, prompted early work (36,37) on the calculation of oxygen balances based on thermodynamic data and detailed post-irradiation examination of irradiated fuels. This field, however, is extremely complicated, and associated with experimental difficulties. Matzke (38) has recently presented a concise review of previous work which can be consulted for further details.

Matzke et al (38) also report the results of recent measurements of $\Delta G(O_2)$ on small fuel fragments of high burnup UO_2 using a minature galvanic cell. The specimens were taken from the pellet centre (burnup 75 MWd/kgU), and from the pellet rim (burnup higher than 200 MWd/kgU), where changes in the local stoichiometry could be most expected. The results showed that the oxide potentials at both positions were extremely low, and that the stoichiometries were similar to that of nominally stoichiometric unirradiated UO_2 examined in the same experimental series. According to the authors, the results can be explained by the oxygen-sink behaviour of the clad (an inner-wall oxide thickness of 15-20 microns was measured) and that about one third of the molybdenum inventory was in the oxidized state.

3.3 MIGRATION, RELEASE AND REDISTRIBUTION

The radial variation of the **formation** of fission products (burnup) and actinides in fuel pellets as a result of the physical processes of fission and neutron capture was discussed in section 3.1. Their distributions in fuel pellets and rods during reactor operation, and therefore in spent fuel, are, however, also determined by chemical effects, and by thermal diffusion and mass transport processes caused by the axial and radial temperature gradients in the fuel rod.

Changes in the oxygen potential of the fuel with increasing burnup, and its radial variation in the fuel, have been discussed briefly in section 3.2 above. Kleykamp (39,40) has published excellent reviews on the chemical state of fission products in oxide fuel, which combine thermodynamic data and phase diagram work with extensive and detailed post-irradiation examination of UO_2 and $(U,Pu)O_2$ fuels. According to Kleykamp, the fission products can be allocated to four main groups with respect to their behaviour in oxide fuels, as is shown in Table 3-1.

Table 3-1. Group classification of fission products in irradiated fuel.

1. Fission gases and other volatile fission products.
Kr, Xe, Br and I.

2. Fission products forming metallic precipitates.
Mo, Tc, Ru, Rh, Pd, Ag, Cd, In, Sn, Sb and Te.

3. Fission products forming oxide precipitates.
Rb, Cs, Ba, Zr, Nb, Mo and Te.

4. Fission products dissolved as oxides in the fuel matrix.
Sr, Zr, Nb, and the rare earths; Y, La, Ce, Pr, Nd, Pm, Sm and Eu.

In operating oxide reactor fuel, however, there are numerous transitions and partitions between the groups (particularly groups 2 and 3) due to the irradiation history (local fuel temperatures) and burnup (solubility restrictions and stoichiometry changes). Further, as a result of beta decay, fission products change their chemical identity both during and subsequent to irradiation.

Although the continuous development and refinement of analytical methods for the quantitative post-irradiation examination of spent fuel has produced great improvements with regard to detection limits and lateral resolution, it is probable that currently available methods cannot quantitatively define these effects in "normal" LWR spent fuel (i.e., medium burnup and with an irradiation history typical of most fuel) to the degree that is necessary for unambiguous interpretation of the results of corrosion tests. Such tests often

have the aim of defining and quantifying the various corrosion processes which occur during both the short- and long-term exposure of spent fuel to groundwater. They therefore often follow analytically not only those nuclides which have direct relevance for safety analysis, but also nuclides which could serve as monitors of corrosion processes under conditions of uranium saturation, as in semi-static tests. This will be discussed further below.

In LWR fuel, the lanthanides and actinides are considered to form stable solid solutions with the UO_2 matrix and are, therefore, available for release to the corrodant groundwater at a rate determined by the corrosion of the matrix. Their solubilities in typical high pH bicarbonate groundwaters, (the corrodant mainly used hitherto in the SKB programme), however, are very low, which prevents their use as corrosion rate monitors.

The chemical states in oxide fuel of the lanthanides and most of the other fission products will not be considered in further detail here since, as mentioned above, the thermodynamic and experimental backgrounds are covered fully in the Kleykamp review (39).

However, in the following, the distributions in spent fuel of Cs, Rb, I, Sr, Ba and Tc, will be briefly discussed against the background of results of corrosion tests on spent fuel. The current view of most workers in this field is that corrosion occurs by three chronologically overlapping processes:

a). The rapid dissolution of fission products released to the fuel and clad surfaces during reactor operation. This applies mainly to cesium and iodine nuclides which are well known to show release behaviour similar to the inert gases, Kr and Xe, so that fission gas release models can be applied to estimate the size of the effect.

b). Selective attack, oxidative or non-oxidative, at the sites of fission product segregations, or at grain boundaries.

c). General matrix dissolution, oxidative or non-oxidative, with the simultaneous release of fission products and actinides to the aqueous phase.

During the corrosion of LWR spent fuel in groundwaters, by far the largest part of all fission product and actinide inventories will be made available for release only by dissolution of the fuel matrix, since only minor fractions of a few nuclides are subjected during irradiation to redistribution processes. However, during corrosion tests, particularly in the sequential static tests often used, the first two processes are dominant for redistributed species over the first few years of water contact. This causes difficulties in the evaluation of test results, since, as stated above, all three processes overlap chronologically. Further, the corrosion of spent fuel in bicarbonate groundwaters is slow. Although the cumulative release to the groundwater of cesium and iodine nuclides during the first few weeks is of the same order as the fission gas release from the fuel (about 1% in the SKB programme reference fuels), the cumulative release of Sr-90, for example, which has been

tentatively used as a monitor of matrix dissolution, is only about 0.1% of the fuel inventory after several years of corrosion under oxic conditions.(30)

The detection and measurement of such small amounts of strontium in spent fuel by post-irradiation examination methods, requires that substantial local enrichment has occured during irradiation. Kleykamp (39) reports that although strontium exists in fuel predominantly dissolved as the oxide (See Table 3-1), it can also be a component in perovskite oxide phases. This effect, however, appears to be more likely in mixed oxide fuel, since strontium partitioning appears to be favoured by decreasing local oxygen potential of the fuel. Attempts to detect and measure Sr gradients in individual grains in power-ramped UO_2 fuel by EPMA (27) were unsuccessful, since the Sr concentrations were of the same order as the detection level.

Nevertheless, the need for more clarity regarding the source terms for the 3 corrosion processes mentioned above, and their dependence on fuel irradiation histories, has prompted a great deal of experimental work during the last few years (41-45), with the aims of direct identification of fission product species on grain surfaces, and quantification of grain boundary inventories. This work is still in progress.

The recent application of the ICP-MS technique to solutions of actinides and fission products, offers another method of studying the different release behaviours of groups of fission products which are mobile in operational fuel, and, therefore, indirectly, their distributions between segregations or zones of enhanced concentration, and the fuel matrix. Thus, in the group Cs, Rb, Sr and Ba, all of which are readily measurable in corrodant solutions by ICP-MS, at least under oxic conditions, the fractional release rates during the early stages of corrosion should reflect their differences in migrational behaviour. At a later stage, as grain boundary segregations are removed by selective attack, the values of fractional release rates should tend to converge, as matrix dissolution becomes the dominant mode of corrosion.

Rubidium, for example, shows the same type of release behaviour as Cs, but to a lesser extent (29,45), while barium has been reported to migrate radially up the temperature gradient (46), and axially along the pellet stack (47). The radial redistribution process has been modelled (48). Further, the isotopic analysis capability of the ICP-MS technique gives the possibility of studying isotopic effects in operational fuel such as the postulated enrichment at grain boundaries of Sr-90 due to the diffusion of its short-lived Br and Rb precursors (42).

The corrodant solutions from the first four years of corrosion of the fuel specimens in the Variable Burnup/Variable Linear Heat Rating Experiment mentioned earlier in this report have been analyzed by the ICP-MS technique, and, although evaluation of the results has not yet been completed, a preliminary assessment suggests that a tendency to release rate convergence can be observed (49).

The fractional release rates of Tc-99 from spent fuel to bicarbonate groundwaters under oxic conditions has been shown to be roughly constant with increasing exposure time, and a similar behaviour is observed for molybdenum (30,49). Under the same conditions, the solution concentrations of the other components of the 4d metal particles, Ru, Rh and Pd, are very low. Since, in the sequential static corrosion tests used in the SKB programme, the fractional release rates for the alkali metal and alkaline earth fission products discussed above decrease rapidly with exposure time, after a few years the Tc-99 release rate is the largest measurable.

Clearly, the source term for Tc-99 release differs in kind from those of the other nuclides, and is attributed to the metal particles observable at grain boundaries and fission gas bubble sites in spent fuel, and therefore readily available for water contact and corrosion.

The composition of these particles and possibly their corrosion resistance, however, should be dependent on the local oxidation potential (38, 39), since at low oxidation potentials Mo exists in the metallic form, while at high potentials, which are thermodynamically predicted at higher burnups towards the fuel pellet centre where most metallic particles are observed, the Mo is oxidized to the hexavalent form and dissolves in the fuel matrix. Thus, Mo is assigned to both groups 2 and 3 in Table 3-1.

As part of the characterization work on the BWR and PWR reference fuels (2), the volume fractions of the metallic particles were estimated by quantitative image analysis during optical microscopic examination of polished fuel cross-sections. Only particles of diameter 0.5 microns and higher could be measured due to the resolution limitations of the microscope. It was found that the measured volume fractions in both fuels corresponded to approximately 0.1 mg/g bulk fuel, which is only about 1% of the combined inventories of Mo, Tc, Ru, Rh and Pd as calculated by ORIGEN-2.

From examinations of spent fuel by analytical transmission electron microscopy and Auger electron spectrometry (50-52), however, the presence at and near grain boundaries of metallic particles with diameters of the order of tens of nanometres has been reported.

An experimental programme has been performed at Studsvik Nuclear's Hot Cell Laboratory (26) in order to estimate the total amounts of 4d metal particles, i.e., including these submicron particles, in the BWR and PWR reference fuels. 4 whole pellet specimens of each fuel were dissolved in cold 6M HNO_3, with an acid/fuel ratio of 30 L/kg fuel. The heavy black residues were filtered through glass biological filters with nominal apertures of 1.0-1.6 microns, and air-dried to constant weight.

Residue weights of 4.54 +/- 0.43 and 4.54 +/- 0.23 mg/g fuel were obtained for the BWR and PWR fuels respectively. The filtrates were also analyzed in order to determine the mass balances. The residues were examined by gamma spectrometry, and, following this, flakes of the residue were mounted on plastic tape for examination by SEM/EPMA.

Figure 3-11 shows a flake from the BWR fuel. EPMA-WDS examination of the upper and lower surfaces of flakes from both fuels showed no significant compositional differences, suggesting that no segregation had occurred during filtration. Further, detailed examination of the residue flakes at higher magnification (see, for example Figure 3-12) showed that the residue was composed of agglomerates of particles of a wide range of sizes, from about a micron down to about 50 nm.

Evaluation of the mass balances showed that about 80% (BWR) and 86% (PWR) of the residues consisted of the 4d metals. Minor components were uranium, actinides, Cs, Sr, Sb and Co.

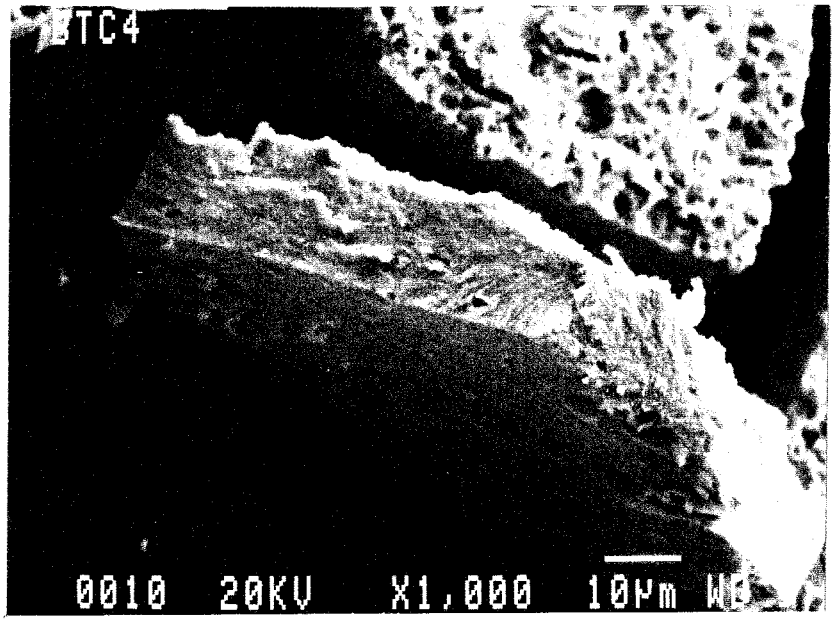

Figure 3-11. *Residue flakes from the BWR reference fuel.*

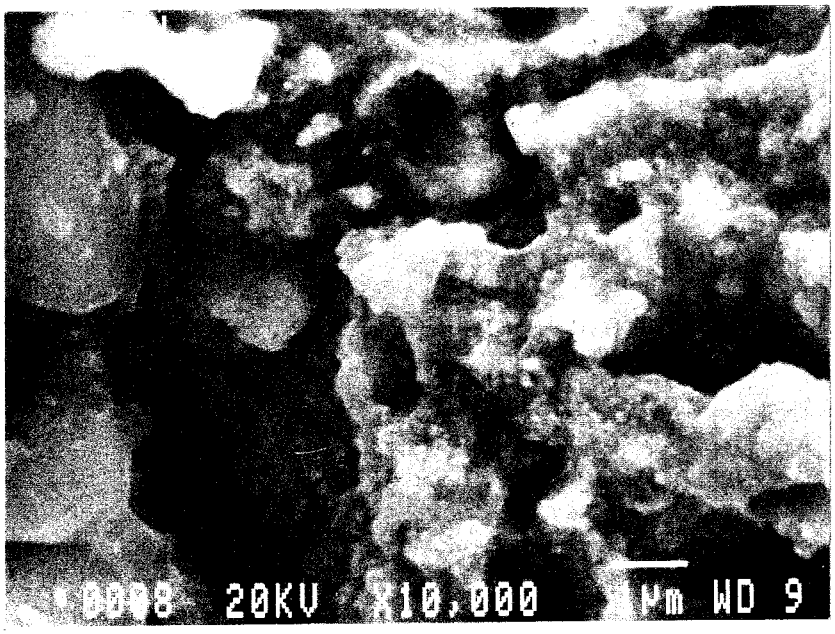

Figure 3-12. *Detail of a BWR residue flake showing submicron particles.*

A similar experiment has been performed by Kleykamp (53) on PWR fuel with an average burnup of 55.9 MWd/kgU. Here, one of the main interests was the composition of dissolver residues during reprocessing operations, and the fuel specimens were dissolved by immersion in 7M HNO_3 at 115 C for five hours. The acid/fuel ratio was 4.5 L/kg fuel. Filtration of the residues was two-stage, through filters of nominal aperture 3 and 1 microns respectively. 91 % of the total residue was found in the 1-3 micron size fraction.

The original paper should be consulted for details of the results obtained, but it is interesting here to make a short comparison with the Studsvik results. After correction for components from structural materials (4.9 wt%), minor components from the fuel (18.5 wt%), and oxygen (12.4 wt%), it is found that the 4d metal (Mo, Tc, Ru, Rh and Pd) content in the residue from the 55.9 MWd/kgU fuel represented 3.85 mg/g fuel, a value similar to the values of 3.63 and 4.21 mg/g fuel obtained for the SKB BWR and PWR reference fuels respectively.

The normalized compositions of the 4d metals in the three residues,are presented in Table 3-2, and the percentages of the calculated total inventories of each element in Table 3-3.

Table 3-2. Comparison of the 4d metal compositions.

Weight %

Fuel	Mo	Tc	Ru	Rh	Pd
SKB: BWR	18.7	9.3	54.8	7.0	10.2
SKB: PWR	20.4	10.4	52.2	7.2	9.8
PWR: (Ref. 53)	23.4	6.4	53.3	6.9	10.1

Table 3-3. Percentage of inventory in the residues.

%

Fuel	Mo	Tc	Ru	Rh	Pd
SKB: BWR	19	42	79	55	20
SKB: PWR	22	52	81	62	21
PWR: (Ref. 53)	19	25	60	51	15

Inspection of these tables shows that there is great similarity between the residues from the 3 fuels, with the exception of the Tc results, where the percentage of the inventory found in the residue in the Kleykamp experiment is significantly lower than for the SKB reference fuels.

On the basis of XRD measurements, Kleykamp states that only about 10% of the residues consisted of undissolved metal particles, while the remainder consisted of oxides or oxide hydrates reprecipitated from the dissolver solution. XRD analysis of the residues from the SKB reference fuels showed that these also were predominantly amorphous. However, from the particle size distribution observed in these latter residues, it is possible that conversion of the metal particles to oxide/oxide hydrates occurred directly, since the dissolution conditions were very dissimilar.

From the discussion above, it is clear that this type of experiment cannot give conclusive data regarding the Tc-99 source term for aqueous corrosion, or even the fraction of the Tc inventory in the metal particles for a particular specimen of spent fuel. If the residues from all 3 fuels were formed predominantly by precipitation from solution, then their composition and amount has little relevance for estimating the Tc source term for spent fuel corrosion. If, however, the residues represent approximately the original particle morphologies, the results can be used as rough measures of Tc grain boundary inventories.

The experiment and its results, however, can serve as a useful illustration of the limitations which govern the experimental determination, and definition, of fission product distributions at the micron and submicron levels in spent fuel.

REFERENCES

1. **Plan 94. 1994** Costs for management of the radioactive waste from nuclear power production.
SKB Technical Report TR 94-23.

2. **Forsyth, R.S. 1987.** Fuel rod D07/B15 from Ringhals 2 PWR. Source material for corrosion/leach tests in groundwater. Fuel rod/pellet characterization program. Part 1.
SKB Technical Report TR 87-02.

3. **Barner, J.O. 1985.** Characterization of LWR Spent Fuel MCC Approved Testing Material-ATM-101.
Report PNL-5109 Rev.1.

4. **Guenther, R.J., Blahnik, D.E., Campbell, T.K., Jenquin, U.P., Mendel, J.E., Thomas, L.E., and Thornhill, C.K. 1988.** Characterization of Spent Fuel Approved Testing Material- ATM-103.
Report PNL-5109-103.

5. **Guenther, R.J., Blahnik, D.E., Jenquin, U.P., Mendel, J.E., Thomas, L.E., and Thornhill, C.K. 1991.** Characterization of Spent Fuel Approved Testing Material- ATM-104.
Report PNL-5109-104.

6. **Guenther, R.J., Blahnik, D.E., Campbell, T.K., Jenquin, U.P., Mendel, J.E., Thomas, L.E., and Thornhill, C.K. 1991.** Characterization of Spent Fuel Approved Testing Material- ATM-105.
Report PNL-5109-105.

7. **Guenther, R.J., Blahnik, D.E., Campbell, T.K., Jenquin, U.P., Mendel, J.E., Thomas, L.E., and Thornhill, C.K. 1991.** Characterization of Spent Fuel Approved Testing Material- ATM-106.
Report PNL-5109-106.

8. **Forsyth, R.S. 1986**. The Hot Cell Laboratory: A short description of programs, facilities and techniques.
Studsvik Nuclear Report. STUDSVIK/NF(P)-86/29.

9. **Forsyth, R.S. and Lysell,G. 1984.** PIE techniques used in the Studsvik Hot Cells for analyzing different stages of fuel rod defects.
Proceedings of the I.A.E.A. Specialist's Meeting on Post-Irradiation Examination and Experience. Tokyo, Japan. 26-30 November 1984.

10. **Ollilla, K. 1990.** Dissolution studies of UO_2 pellets and powdered UO_2.
Technical Report TVO/KPA 90-06. (In Finnish)

11. Gray, W.J., Thomas, L.E. and Einziger, R.E. 1993. Effects of air oxidation on the dissolution rate of LWR spent fuel.
Mat. Res. Soc. Symp. Proc. Vol. 294, 47-54 (1993)

12. Grambow, B., Loida, A., Dressler, P., Geckeis, H., Diaz, P., Gago, J., Casas, L., de Pablo, J., Gimenes, J. and Torrero, M.E. 1994. Reaction of high burnup spent fuel and UO_2 in saline brines at room temperature.
Kernforschungszentrum Karlsruhe Report KfK 5377.

13. Lundström, M., Eklund, U-B. and Forsyth, R.S. 1995.
Studsvik Nuclear Report. To be published.

14. Gray, W.J. and Thomas, L.E. 1994. Initial results from dissolution testing of various air-oxidized spent fuels.
Mat. Res. Soc. Symp. Proc. Vol. 333, 391-398 (1994).

15. Mendelson, M.I. 1969. Average grain size in polycrystalline ceramics.
J. Amer. Ceram. Soc., 52, 443-446.

16. ASTM Standard Method E 321-79 (Reapproved 1990) Standard Test Method for Atom Percent Fission in Uranium and Plutonium Fuel. (Neodymium-148 Method)

17. Barner, J.O., Cunningham, M.E., Freshley, M.D. and Lanning, D. 1991. Relationship between microstructure and fission gas release in high burnup UO_2 fuel with emphasis on the rim region.
Proceedings of the ANS/ENS International Topical Meeting on LWR Fuel Performance. Vol 2, 538-548. Avignon, France. 21-24 April 1991.

18. Walker, C.T. and Coquerelle, M. 1991. Correlation between microstructure and fission gas release in high burnup UO_2 and MOX fuel.
Ibid. 506-517.

19. Walker. C.T., Kameyama, T., Kitajima, S. and Kinoshita, M. 1992. Concerning the microstructure changes that occur at the surface of UO_2 pellets on irradiation to high burnup.
J. Nucl. Mater. 188 73-79. 1992

20. Kameyama, T., Matsumura, T. and Kinoshita, M. 1991. Analysis of rim structure formation in Batelle High Burnup Effects Program.
Proceedings of the ANS/ENS International Topical Meeting on LWR Fuel Performance. Vol 2, 620-626. Avignon, France. 21-24 April 1991.

21. Barner, J.O., Cunningham, M.E., Freshley, M.D. and Lanning, D. 1993. Evaluation of fission gas release in high burnup light water reactor fuel rods. Nucl. Technology. 102. 210-230. 1993

22. Evaluation of spent fuel as a waste form.
Technical Report Series No. 320 (IAEA, Vienna, 1991)

23. Forsyth, R.S. and Mattsson,O. Unpublished results.

24. Matzke, Hj. 1992. On the rim effect in high burnup UO_2 LWR fuels. J. Nucl. Mater. 189 (1992) 141-148.

25. Institute for Transuranium Elements. Annual Report 1993. EUR 15741 EN. 19-24.

26. Forsyth, R.S. 1990. The application of PIE techniques to the study of the corrosion of spent oxide fuel in deep-rock groundwaters. SKB Technical Report TR 91-03.

27. Forsyth, R.S., Mattsson, O. and Schrire, D. 1988. Fission product concentration profiles (Sr, Xe, Cs and Nd) at the individual grain level in power-ramped LWR fuel. SKB Technical Report TR 88-24.

28. Forsyth, R.S., Gustafsson, I. and Nilsson, B. Unpublished results.

29. Forsyth, R.S., Eklund, U-B. and Werme, L.O. 1994. A study of fission product migration and selective leaching by means of a power-bump test. Mat. Res. Soc. Symp: Proc. Vol. 333. 1994

30. Forsyth, R.S. and Werme, L.O. 1992. Spent fuel corrosion and dissolution. J. Nucl. Mater. 190. (1992) 3-19.

31. Garcia Alonso, J. I., Garcia Serrano, J., Babelot, J.-F., Closset, J.-C., Nicolaou, G. and Koch, L. 1993. Laser ablation ICP-MS on spent nuclear fuel. Applications of Plasma Source Mass Spectrometry II. Ed. G. Holland and A.N. Eaton, Royal Society of Chemistry, London.

32. Forsyth. R.S. 1993. Corrosion sites in high burnup fuel: Pellet rim or bulk fuel? Overhead presentation. Spent Nuclear Fuel Workshop, Santa Fe, N.M., U.S.A. 27-29 Sept. 1993.

33. SKB Annual Report 1993. SKB Technical Report 93-34. 73-76. 1994.

34. Forsyth, R.S., Eklund, U-B. and Mattsson, O. Unpublished results.

35. Forsyth, R.S. and Eklund, U-B. 1995. Spent nuclear fuel corrosion: The application of ICP-MS to direct actinide analysis. Proceedings of the 4th International Conference on Plasma Source Mass Spectrometry, Durham, England. 11-16 Sept. 1994.

36. Davies, J.H. and Ewart, F.T. 1971. The chemical effects of composition changes in irradiated oxide fuel materials,
J. Nucl. Mater. 41 (1971) 143-155.

37. Ewart, F.T., Taylor, R.G., Horspool, J.M. and James, G. 1976. The chemical effects of composition changes in irradiated oxide fuel materials. II- Fission product segregation and chemical equilibria.
J. Nucl. Mater. 61 (1976) 254-270.

38. Institute for Transuranium Elements. Annual Report 1993.
EUR 15741 EN. 24-30.

39. Kleykamp, H. 1985. The chemical state of the fission products in oxide fuels.
J. Nucl. Mater. 131 (1985) 221-246.

40. Kleykamp, H. 1988. The chemical state of fission products in oxide fuels at different stages of the nuclear fuel cycle.
Nucl. Technology. Vol 80 (1988) 412-422.

41. Stroes-Gascoyne, S. and Selinger D.M. 1986. The effect of fuel power on the leaching of cesium and iodine from used CANDU fuel.
Proc. of the First Int. Conf. on CANDU Fuel. Chalk River, Canada, 6-8 Oct. 1986. (Ed. Hastings, I.J.)

42. Garisto, N.C., Johnson, L.H. and Hocking, W.H. 1989. An Instant-Release Source Term for the assessment of used nuclear fuel disposal.
Proc. of the Second Int. Conf. on CANDU Fuel. Chalk River, Canada, 1-5 Oct. 1989. (Ed. Fehrenbach, P.J. and Hastings, I.J.)

43. Gray, W.J. and Strachan, D.M. 1991. UO_2 matrix dissolution rates and grain boundary inventories of Cs, Sr and Tc in spent LWR fuel.
Mat. Res. Soc. Symp. Proc. Vol. 212, 205-212 (1991).

44. Gray, W.J., Strachan, D.M. and Wilson, C.N. 1992. Gap and grain boundary inventories of Cs, Tc and Sr in spent LWR fuel.
Mat. Res. Soc. Symp. Proc. Vol. 257, 353-360 (1992).

45. Hocking, W.H., Duclos, M. and Johnson, L.H. 1994. Study of fission product segregation in used CANDU fuel by X-ray photoelectron spectroscopy (XPS) II.
J. Nucl. Mater. 209 (1994) 1-26.

46. Forsyth, R.S., Blackadder, W.H. and Nilsson, B. 1976. Volatile fission product behaviour in reactor fuel under accident conditions.
Proc. of the CSNI Specialist Meeting on the Behaviour of Water Reactor Fuel Elements under Accident Conditions. Spåtind (Norway) 12-16 Sept. 1976.

47. Walker, C.T., Bagger, C. and Mogensen, M. 1990. Migration of fission product Barium in UO_2 fuel under transient conditions.
J. Nucl. Mater. 173 (1990) 14-25.

48. Malen, K. 1980. FIPMIGR- A computer program for studying migration of fission products in a temperature gradient.
Nucl. Engineering and Design. 56 (1980) 177-181.

49. Forsyth, R. S. and Eklund, U-B. 1995. To be published.

50. Thomas, L. E., Einziger, R. E. and Woodley, R. E. 1989. The microstructural examination of oxidized spent PWR fuel by transmission electron microscopy.
J. Nucl. Mater. 166 (1989) 243-251.

51. Thomas. L. E., Beyer, C. E. and Charlot, L.A. 1992. Microstructural analysis of LWR spent fuels at high burnup.
J. Nucl. Mater. 188 (1992) 80-89.

52. Ray, I. L. F., Thiele, H. and Matzke, Hj. 1992. Transmission electron microscopy study of fission product behaviour in high burnup UO_2.
Ibid. pp 90-95.

53. Kleykamp, H. 1990. Post-irradiation examinations and composition of the residues from nitric acid dissolution experiments of high-burnup LWR fuel.
J. Nucl. Mater. 171 (1990) 181-188.

List of SKB reports

Annual Reports

1977-78
TR 121
KBS Technical Reports 1 – 120
Summaries
Stockholm, May 1979

1979
TR 79-28
The KBS Annual Report 1979
KBS Technical Reports 79-01 – 79-27
Summaries
Stockholm, March 1980

1980
TR 80-26
The KBS Annual Report 1980
KBS Technical Reports 80-01 – 80-25
Summaries
Stockholm, March 1981

1981
TR 81-17
The KBS Annual Report 1981
KBS Technical Reports 81-01 – 81-16
Summaries
Stockholm, April 1982

1982
TR 82-28
The KBS Annual Report 1982
KBS Technical Reports 82-01 – 82-27
Summaries
Stockholm, July 1983

1983
TR 83-77
The KBS Annual Report 1983
KBS Technical Reports 83-01 – 83-76
Summaries
Stockholm, June 1984

1984
TR 85-01
Annual Research and Development Report 1984
Including Summaries of Technical Reports Issued during 1984. (Technical Reports 84-01 – 84-19)
Stockholm, June 1985

1985
TR 85-20
Annual Research and Development Report 1985
Including Summaries of Technical Reports Issued during 1985. (Technical Reports 85-01 – 85-19)
Stockholm, May 1986

1986
TR 86-31
SKB Annual Report 1986
Including Summaries of Technical Reports Issued during 1986
Stockholm, May 1987

1987
TR 87-33
SKB Annual Report 1987
Including Summaries of Technical Reports Issued during 1987
Stockholm, May 1988

1988
TR 88-32
SKB Annual Report 1988
Including Summaries of Technical Reports Issued during 1988
Stockholm, May 1989

1989
TR 89-40
SKB Annual Report 1989
Including Summaries of Technical Reports Issued during 1989
Stockholm, May 1990

1990
TR 90-46
SKB Annual Report 1990
Including Summaries of Technical Reports Issued during 1990
Stockholm, May 1991

1991
TR 91-64
SKB Annual Report 1991
Including Summaries of Technical Reports Issued during 1991
Stockholm, April 1992

1992
TR 92-46
SKB Annual Report 1992
Including Summaries of Technical Reports Issued during 1992
Stockholm, May 1993

1993
TR 93-34
SKB Annual Report 1993
Including Summaries of Technical Reports Issued during 1993
Stockholm, May 1994

1994

TR 94-33

SKB Annual Report 1994

Including Summaries of Technical Reports Issued during 1994.
Stockholm, May 1995

List of SKB Technical Reports 1995

TR 95-01

Biotite and chlorite weathering at 25°C. The dependence of pH and (bi) carbonate on weathering kinetics, dissolution stoichiometry, and solubility; and the relation to redox conditions in granitic aquifers

Maria Malmström[1], Steven Banwart[1], Lara Duro[2], Paul Wersin[3], Jordi Bruno[3]
[1] Royal Institute of Technology, Department of Inorganic Chemistry, Stockholm, Sweden
[2] Universidad Politécnica de Cataluña, Departmento de Inginería Química, Barcelona, Spain
[3] MBT Tecnología Ambiental, Cerdanyola, Spain
January 1995

TR 95-02

Copper canister with cast inner component. Amendment to project on Alternative Systems Study (PASS), SKB TR 93-04

Lars Werme, Joachim Eriksson
Swedish Nuclear Fuel and Waste Management Co, Stockholm, Sweden
March 1995

TR 95-03

Prestudy of final disposal of long-lived low and intermediate level waste

Marie Wiborgh (ed.)
Kemakta Konsult AB, Stockholm, Sweden
January 1995

TR 95-04

Spent nuclear fuel corrosion: The application of ICP-MS to direct actinide analysis

R S Forsyth[1], U-B Eklund[2]
[1] Caledon-Consult AB, Nyköping, Sweden
[2] Studsvik Nuclear AB, Nyköping, Sweden
March 1995

TR 95-06

Palaeohydrological implications in the Baltic area and its relation to the groundwater at Äspö, south-eastern Sweden – A literature study

Bill Wallin
Geokema AB, Lidingö, Sweden
March, 1995

TR 95-07

Äspö Hard Rock Laboratory Annual Report 1994

SKB
April 1995

TR 95-08

Feasibility study for siting of a deep repository within the Storuman municipality

Swedish Nuclear Fuel and Waste Management Co., Stockholm
January 1995

TR 95-09

A thermodynamic data base for Tc to calculate equilibrium solubilities at temperatures up to 300°C

Ignasi Puigdomènech[1], Jordi Bruno[2]
[1] Studsvik AB, Nyköping, Sweden
[2] Intera Information Technologies SL, Cerdanyola, Spain
April 1995

TR 95-10

Investigations of subterranean microorganisms. Their importance for performance assessment of radioactive waste disposal

Karsten Pedersen[1], Fred Karlsson[2]
[1] Göteborg University, General and Marine Microbiology, The Lundberg Institute, Göteborg, Sweden
[2] Swedish Nuclear Fuel and Waste Management Co., Stockholm, Sweden
June 1995

TR 95-11

Solute transport in fractured media – The important mechanisms for performance assessment

Luis Moreno, Björn Gylling, Ivars Neretnieks
Department of Chemical Engineering and Technology, Royal Institute of Technology, Stockholm, Sweden
June 1995

TR 95-12

Literature survey of matrix diffusion theory and of experiments and data including natural analogues

Yvonne Ohlsson, Ivars Neretnieks
Department of Chemical Engineering and Technology, Royal Institute of Technology, Stockholm, Sweden
August 1995

TR 95-13

Interactions of trace elements with fracture filling minerals from the Äspö Hard Rock Laboratory

Ove Landström[1], Eva-Lena Tullborg[2]
[1] Studsvik Eco & Safety AB
[2] Terralogica AB
June 1995

TR 95-14

Consequences of using crushed crystalline rock as ballast in KBS-3 tunnels instead of rounded quartz particles

Roland Pusch
Clay Technology AB
February 1995

TR 95-15

Estimation of effective block conductivities based on discrete network analyses using data from the Äspö site

Paul R La Pointe[1], Peter Wallmann[1], Sven Follin[2]
[1] Golder Associates Inc., Seattle, WA, USA
[2] Golder Associates AB, Lund, Sweden
September 1995

TR 95-16

Temperature conditions in the SKB study sites

Kaj Ahlbom[1], Olle Olsson[1], Stefan Sehlstedt[2]
[1] Conterra AB
[2] MRM Konsult AB
June 1995

TR 95-17

Measurements of colloid concentrations in the fracture zone, Äspö Hard Rock Laboratory, Sweden

Anna Ledin, Anders Düker, Stefan Karlsson, Bert Allard
Department of Water and Environmental Studies,Linköping University, Linköping, Sweden
June 1995

TR 95-18

Thermal evidence of caledonide foreland, molasse sedimentation in Fennoscandia

Eva-Lena Tullborg[1], Sven Åke Larsson[1], Lennart Björklund[1], Lennart Samuelsson[2], Jimmy Stigh[1]
[1] Department of Geology, Earth Sciences Centre, Göteborg University, Göteborg, Sweden
[2] Geological Survey of Sweden, Earth Sciences Centre, Göteborg, Sweden
November 1995

TR 95-19

Compaction of bentonite blocks. Development of technique for industrial production of blocks which are manageable by man

Lars-Erik Johannesson, Lennart Börgesson, Torbjörn Sandén
Clay Technology AB, Lund, Sweden
April 1995

TR 95-20

Modelling of the physical behaviour of water saturated clay barriers. Laboratory tests, material models and finite element application

Lennart Börgesson[1], Lars-Erik Johannesson[1], Torbjörn Sandén[1], Jan Hernelind[2]
[1] Clay Technology AB, Lund, Sweden
[2] FEM-Tech AB, Västerås, Sweden
September 1995

TR 95-21

Conceptual model for concrete long time degradation in a deep nuclear waste repository

Björn Lagerblad, Jan Trägårdh
Swedish Cement and Concrete Research Institute
February 1994

TR 95-22

The use of interaction matrices for identification, structuring and ranking of FEPs in a repository system. Application on the far-field of a deep geological repository for spent fuel

Kristina Skagius[1], Anders Ström[2], Marie Wiborgh[1]
[1] Kemakta, Stockholm, Sweden
[2] Swedish Nuclear Fuel and Waste Management Co, Stockholm, Sweden
November 1995